Monthly Notices
of the
ROYAL ASTRONOMICAL SOCIETY

MNRAS **430,** 869–887 (2013) doi:10.1093/mnras/sts609

Photometric and spectroscopic evolution of supernova SN 2009an: another case of a transitional Type Ia event

D. K. Sahu,⋆ G. C. Anupama⋆ and P. Anto

Indian Institute of Astrophysics, Koramangala, Bangalore 560 034, India

Accepted 2012 December 11. Received 2012 December 6; in original form 2012 May 29

ABSTRACT

We present optical *UBVRI* photometry and medium-resolution spectroscopy of a transitional Type Ia supernova, SN 2009an, over the period −6 to ∼+150 d from the *B* maximum. With a $\Delta m_{15}(B) = 1.514 \pm 0.132$, SN 2009an declines faster than normal Type Ia events, but slower than the fast-declining, low-luminosity 1991bg-like events. The *B*-band absolute magnitude at maximum is -19.02 ± 0.20. The peak bolometric luminosity indicates that 0.41 $M_\odot$ of ^{56}Ni was synthesized during the explosion. The pre-maximum and early post-maximum spectral evolution of SN 2009an is very similar to that in the transitional Type Ia SN 2004eo. High-velocity features in the Ca II near-infrared triplet are seen during the early phases. Similar to the other few objects belonging to this class, SN 2009an exhibits a higher value (∼0.4) of the Si II line ratio *R*(Si II). The velocity gradient of the Si II 6355 Å line in the post-maximum epoch ($\dot{v} = 60\,\mathrm{km\,s^{-1}\,d^{-1}}$) is at the boundary between the low-velocity-gradient and high-velocity-gradient groups.

Key words: techniques: photometric – techniques: spectroscopic – supernovae: general – supernovae: individual: SN 2009an.

1 INTRODUCTION

Type Ia supernovae (SNe Ia) are the result of the thermonuclear explosion of CO white dwarfs with mass close to the Chandrasekhar limit ($M \sim M_{\rm ch}$). Because of their almost identical progenitor systems, SNe Ia were thought to belong to a homogeneous class. In a volume-limited sample, the majority of SNe Ia (∼70 per cent) belong to a fairly homogeneous class termed 'normal' Type Ia; ∼9 per cent belong to the class of overluminous SN 1991T-like objects; ∼15 per cent belong to the class of underluminous SN 1991bg-like objects; and ∼5 per cent belong to the class of peculiar SN 2002cx-like objects (Li et al. 2011). The high quality of observational data accumulated during the last decade has unambiguously demonstrated that, photometrically, SNe Ia have a wide range of light-curve-shape parameters, for example $\Delta m_{15}(B)$ (Phillips 1993), stretch factor '*s*' (Goldhaber et al. 2001), luminosity and mass of ^{56}Ni synthesized in the explosion (Contardo et al. 2000). Similarly, spectroscopically there is a wide range in the expansion velocity and its gradients (Benetti et al. 2005, Blondin et al. 2012), and in the ratio of the depth of some prominent lines, for example *R*(Si II) (Nugent et al. 1995; Blondin et al. 2012). They are, however, considered as standard candles, thanks to the empirical relationships between peak luminosities and the shape of the light curve (Phillips 1993; Hamuy et al. 1996; Riess, Pree & Kirshner 1996; Phillips et al. 1999; Goldhaber et al. 2001; Wang et al. 2003). There are more recent methods, for example SALT (Guy et al. 2005) and SALT2 (Silverman et al. 2012), which measure a parametrization of the light-curve width (*x*1), the supernova colour (*c*) and the apparent *B*-band magnitude at maximum light (m_B). There are some spectroscopic luminosity indicators also, such as the ratio of the depth of two absorptions at 5800 and 6100 Å (Nugent et al. 1995; Benetti et al. 2005), which is found to anti-correlate with the absolute magnitude, and the equivalent widths of lines due to intermediate-mass elements such as Si II λ6355, which are found to be larger-valued for intermediate decliners and smaller for bright and faint objects. The O I λ7773 line is found to be strong in fainter supernovae and tends to become weaker with increasing luminosity (Hachinger, Mazzali & Benetti 2006). Recently, Bronder et al. (2008) found that the equivalent width of Si II λ4130 is anti-correlated with the peak *B*-band absolute magnitude. Extending to the light-curve stretch factor '*s*', Walker et al. (2011) and Silverman et al. (2012) showed that the high-stretch (brighter) objects have a lower Si II λ4130 equivalent width. Foley, Sanders & Kirshner (2011) found that the maximum light velocity of Si II λ6355 and Ca II H&K, and the maximum light pseudo-equivalent-width of Si II λ6355 are strongly correlated with the intrinsic ($B - V$) colour at peak brightness. However, Blondin et al. (2012) reported a weaker and less significant correlation between the Si II velocity and intrinsic ($B - V$) colour, while Maguire et al. (2012) and Silverman et al. (2012) found no correlation between the Ca II H&K velocity and the intrinsic ($B - V$) colour.

⋆ E-mail: dks@iiap.res.in (DKS); gca@iiap.res.in (GCA)

In addition to the basic explosion characteristics that determine the properties of SNe Ia, the environment and the type of host galaxy also influence the observed properties. The luminosity of a SN Ia depends on the morphological type of the host galaxy. SNe Ia hosted by early-type E/SO galaxies are fainter than those in spiral galaxies, indicating that brighter events occur preferentially in younger stellar environments (Reindl et al. 2005; Hamuy et al. 2000). This dependence led Mannucci et al. (2005) to propose the existence of two populations of progenitors: (i) those found in late-type star-forming spirals and associated with a relatively younger stellar population, and (ii) those related to old stars in early-type E/SO galaxies. This is also expressed in terms of the difference in the delay times for progenitor formation to explosion in the two environments. From the observed bimodal distribution of delay time for SNe Ia, it is expected that the bright SNe Ia events are preferentially associated with the 'prompt' population, which is more common in spiral and irregular galaxies, while the faint and rapidly decaying objects are more easily found in the 'tardy' component, which is more common in early-type galaxies (Mannucci, Della Valle & Panagia 2006).

SNe Ia with a relatively high Δm_{15}(B), relatively low ejecta velocity, moderate velocity gradient and peculiar evolution of the R(Si II) line ratio have been termed non-standard or transitional Type Ia events (Pastorello et al. 2007). They have a fainter absolute B maximum and produce less ^{56}Ni than normal SNe Ia. They are supposed to bridge the gap between the 'normal' and the fainter SN 1991bg-like events. This is a rare class, with only a few well-studied objects, namely SN 2003hv (Leloudas et al. 2009), SN 2004eo (Pastorello et al. 2007), SN 1992A (Kirshner et al. 1993) and SN 1989B (Wells et al. 1994). Detailed studies of more objects belonging to this class are required in order to gain an understanding of the properties of these transitional types of SNe Ia.

Supernova SN 2009an was discovered by Cortitini & Antonellini (2009) on 2009 February 27.93 at an unfiltered magnitude of ∼15.4 in the barred spiral galaxy NGC 4332. An independent discovery of SN 2009an at magnitude ∼15.6 was reported by Kehusmaa (2009). Based on a spectrum obtained on 2009 February 28, Challis (2009) classified SN 2009an as a normal Type Ia supernova, about 5 d before maximum. Yamanaka & Arai (2009) and Vinko et al. (2009) reported the presence of a high-velocity component in the Ca II infrared triplet at ∼22 500 km s^{-1}, in the early spectra obtained around March 1.5.

Detailed photometric and spectroscopic observations, covering the early as well as the late phase of SN 2009an, are presented in this paper.

2 OBSERVATIONS AND DATA REDUCTION

2.1 Photometry

The monitoring of SN 2009an with the 2-m Himalayan Chandra Telescope (HCT) of the Indian Astronomical Observatory (IAO), Hanle, India, began on 2009 March 1 (JD 245 4892.35), soon after its discovery, and continued until 2009 August 3 (JD 245 5047.13). It was monitored in the Bessell *UBVRI* bands, using the Himalayan Faint Object Spectrograph Camera (HFOSC) installed on the HCT. The central 2k × 2k pixels of the 2k × 4k pixels SITe CCD chip were used for imaging. With a plate scale of 0.296 arcsec pixel^{-1}, it covers a region of 10 × 10 arcmin^2 of the sky. Standard star fields pg0918+029, pg1047+003, pg1323-086, pg0942-029 and pg1633+099 from the list of Landolt (1992) were observed on the nights of 2009 March 15, 30 and 31 under photometric conditions and were used to calibrate a sequence of secondary standards in the supernova field.

The images were bias-subtracted and flat-field-corrected using various tasks available within IRAF. Aperture photometry was performed on the standard fields, with an aperture 3–4 times the full width at half-maximum (FWHM) of the stellar profile, determined using the aperture growth curve. The average value of atmospheric extinction for the site and the average colour terms for the system were used to determine the photometric zero-points on calibration nights. A sequence of secondary standards was calibrated using the average colour terms and the estimated zero-points. The secondary standards are marked in Fig. 1. The *UBVRI* magnitudes of the sequence of secondary standards in the supernova field, averaged over three nights, are listed in Table 1. The errors in the magnitudes are the standard deviation of the standard magnitudes obtained on the three photometric nights.

The magnitudes of the supernova and secondary standards were estimated using the profile-fitting technique, with a fitting radius close to the FWHM of the stellar profile. The difference between the aperture and profile-fitting magnitudes was obtained using bright stars in the supernova field, and this difference was applied to the supernova magnitude. The standard magnitude of the supernova was obtained differentially with respect to the secondary standards calibrated in the supernova field. The estimated supernova magnitudes in the U, B, V, R and I bands are listed in Table 2. The errors quoted in the magnitude table were estimated by adding in quadrature the errors associated with the nightly photometric zero-point, the error associated with the aperture corrections, and the fitting errors as computed by IRAF.

2.2 Spectroscopy

Spectroscopic observations of SN 2009an were made on 20 epochs during the period 2009 March 1 (JD 245 4892.29) to June 23 (JD 245 5006.18). The spectra were obtained using grisms Gr#7 (wavelength range 3500–7800 Å) and Gr#8 (wavelength range 5200–9250 Å) available with HFOSC. The log of spectroscopic observations is given in Table 3. Arc-lamp spectra of FeNe and FeAr were obtained for wavelength calibration. Spectrophotometric standards Feige 34, Hz 44 and Feige 110, observed with the same setup as the supernova, were used to correct for the instrumental response.

Spectroscopic data reduction was carried out in the standard manner using the tasks available in IRAF. The two-dimensional images were bias-corrected and flat-fielded. The one-dimensional spectrum was extracted using the optimal extraction method. The extracted spectra were wavelength-calibrated using the FeNe (for Grism #8) or the FeAr (for Grism #7) arc spectra obtained soon after the supernova spectrum. The wavelength calibration was checked using the night sky lines. The spectra were corrected for the continuum atmospheric extinction using the mean extinction curve for the site and then corrected for instrumental response using the spectra of the spectrophotometric standards observed on the same night. On the nights when the spectrophotometric standards could not be observed, spectra obtained during nearby nights were used. The spectra in the two different regions were combined and scaled to a weighted mean to give the final spectrum on a relative flux scale, which was then brought to an absolute flux scale using the *UBVRI* magnitudes.

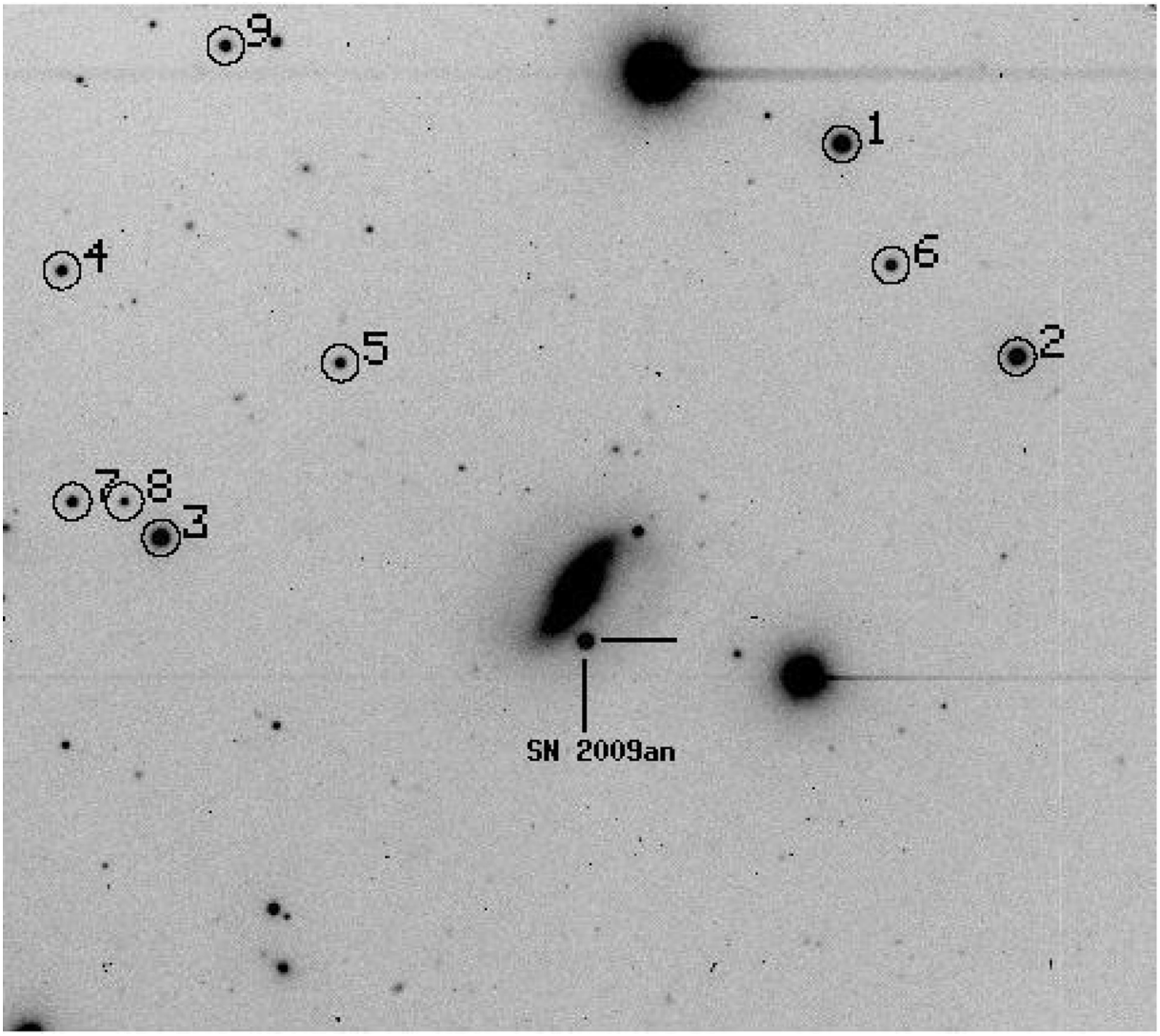

Figure 1. Identification chart for SN 2009an. The stars used as local standards are marked as numbers 1–9. South is up and east is to the right. The field of view is 10×10 arcmin^2.

Table 1. Magnitudes for the sequence of secondary standard stars in the field of SN 2009an. The star IDs are as marked in Fig. 1.

ID	*U*	*B*	*V*	*R*	*I*
1	15.168 ± 0.036	14.894 ± 0.010	14.123 ± 0.001	13.659 ± 0.007	13.243 ± 0.020
2	16.309 ± 0.040	15.411 ± 0.005	14.383 ± 0.002	13.825 ± 0.002	13.347 ± 0.013
3	15.145 ± 0.028	14.991 ± 0.013	14.330 ± 0.007	13.964 ± 0.002	13.617 ± 0.010
4	16.760 ± 0.013	16.770 ± 0.013	16.154 ± 0.007	15.805 ± 0.014	15.452 ± 0.021
5	18.223 ± 0.005	17.287 ± 0.003	16.280 ± 0.004	15.693 ± 0.007	15.194 ± 0.016
6	17.371 ± 0.041	16.791 ± 0.010	15.961 ± 0.003	15.483 ± 0.007	15.088 ± 0.013
7	18.835 ± 0.035	17.565 ± 0.010	16.335 ± 0.006	15.604 ± 0.015	14.927 ± 0.029
8	18.129 ± 0.030	17.979 ± 0.004	17.272 ± 0.007	16.868 ± 0.008	16.471 ± 0.001
9	16.520 ± 0.006	16.468 ± 0.004	15.821 ± 0.002	15.479 ± 0.010	15.109 ± 0.015

3 LIGHT CURVE AND COLOUR CURVES

The *UBVRI* light curves of SN 2009an are presented in Fig. 2. The good photometric coverage of SN 2009an allows us to estimate the light-curve parameters, namely epoch of maximum light in various bands, peak magnitudes, decline-rate parameter soon after the peak Δm_{15}, and the late-phase decline rate. The date of maximum and peak magnitudes were estimated by fitting a low-order polynomial to the points around maximum. Our estimates of the dates of maximum, apparent maximum magnitude and the decline-rate parameters are listed in Table 4. The light-curve fit indicates that the supernova reached a *B*-maximum light of 14.547 ± 0.025 mag on JD 245 4898.5 ± 1. The decline-rate parameter in the *B*-band, $\Delta m_{15}(B)$, is estimated as 1.514 ± 0.132. The maximum in the *V* and

Table 2. Photometric observations of SN 2009an.

Date	JD 245 0000+	Phase* (d)	*U*	*B*	*V*	*R*	*I*
01/03/2009	4892.35	−6.15	14.837 ± 0.029	15.067 ± 0.022	15.062 ± 0.008	14.893 ± 0.005	15.030 ± 0.014
02/03/2009	4893.33	−5.17	14.659 ± 0.013	14.898 ± 0.014	14.899 ± 0.008	14.760 ± 0.007	14.863 ± 0.013
03/03/2009	4894.37	−4.13	14.489 ± 0.033	14.789 ± 0.009	14.807 ± 0.015	14.657 ± 0.012	14.728 ± 0.015
04/03/2009	4895.51	−2.99		14.694 ± 0.021	14.701 ± 0.012	14.551 ± 0.009	14.727 ± 0.011
05/03/2009	4896.33	−2.17	14.447 ± 0.035	14.657 ± 0.025	14.659 ± 0.015	14.540 ± 0.006	14.729 ± 0.012
07/03/2009	4898.11	−0.39	14.613 ± 0.092	14.585 ± 0.042	14.586 ± 0.021	14.466 ± 0.016	14.755 ± 0.011
10/03/2009	4901.36	2.86	14.494 ± 0.035	14.583 ± 0.027	14.525 ± 0.022	14.406 ± 0.019	14.729 ± 0.026
15/03/2009	4906.44	7.94	14.937 ± 0.029	15.082 ± 0.026	14.745 ± 0.012	14.763 ± 0.018	15.171 ± 0.019
19/03/2009	4910.48	11.98	15.513 ± 0.030	15.649 ± 0.016	15.036 ± 0.015	15.099 ± 0.026	15.300 ± 0.011
26/03/2009	4917.28	18.78		16.518 ± 0.009	15.422 ± 0.012	15.209 ± 0.019	15.143 ± 0.015
27/03/2009	4918.25	19.75	16.642 ± 0.008	16.616 ± 0.009	15.473 ± 0.015	15.232 ± 0.012	15.148 ± 0.038
29/03/2009	4920.42	21.92		16.827 ± 0.010	15.577 ± 0.006	15.261 ± 0.011	15.100 ± 0.006
30/03/2009	4921.18	22.68	16.971 ± 0.010	16.891 ± 0.006	15.633 ± 0.006	15.297 ± 0.007	15.120 ± 0.010
31/03/2009	4922.19	23.69	17.030 ± 0.017	17.010 ± 0.023	15.714 ± 0.008	15.358 ± 0.010	15.123 ± 0.014
03/04/2009	4925.10	26.60		17.294 ± 0.021	15.945 ± 0.040	15.544 ± 0.018	15.323 ± 0.024
07/04/2009	4929.12	30.62	17.620 ± 0.043	17.490 ± 0.017	16.280 ± 0.012	15.911 ± 0.017	15.619 ± 0.031
10/04/2009	4932.19	33.69		17.596 ± 0.013	16.422 ± 0.015	16.102 ± 0.008	15.862 ± 0.023
17/04/2009	4939.15	40.65	17.821 ± 0.025	17.820 ± 0.023	16.669 ± 0.007	16.401 ± 0.008	16.270 ± 0.010
24/04/2009	4946.13	47.63	17.963 ± 0.024	17.860 ± 0.016	16.879 ± 0.019	16.677 ± 0.008	16.594 ± 0.018
28/04/2009	4950.21	51.71	17.975 ± 0.015	17.945 ± 0.013	16.958 ± 0.009	16.763 ± 0.008	16.747 ± 0.010
29/04/2009	4951.39	52.89		17.968 ± 0.023	16.996 ± 0.021	16.819 ± 0.018	16.838 ± 0.021
07/05/2009	4959.22	60.72	18.145 ± 0.034	17.996 ± 0.031	17.215 ± 0.016	17.087 ± 0.013	17.136 ± 0.026
12/05/2009	4964.35	65.85	18.308 ± 0.030	18.125 ± 0.025	17.356 ± 0.013	17.298 ± 0.024	17.371 ± 0.025
21/05/2009	4973.19	74.69	18.516 ± 0.018	18.295 ± 0.021	17.597 ± 0.009	17.549 ± 0.010	
22/05/2009	4974.17	75.67	18.568 ± 0.027	18.255 ± 0.015	17.646 ± 0.011	17.599 ± 0.013	17.699 ± 0.021
04/06/2009	4987.20	88.70		18.486 ± 0.056	17.966 ± 0.047	17.829 ± 0.053	18.139 ± 0.052
06/06/2009	4989.24	90.74			18.095 ± 0.027	18.024 ± 0.025	
10/06/2009	4993.13	94.63		18.537 ± 0.054	18.115 ± 0.038	18.180 ± 0.019	18.290 ± 0.027
23/06/2009	5006.14	107.64		18.744 ± 0.018	18.413 ± 0.021	18.524 ± 0.027	18.529 ± 0.045
09/07/2009	5022.14	123.64			18.727 ± 0.012	18.965 ± 0.019	19.095 ± 0.061
22/07/2009	5035.18	136.68		19.250 ± 0.018	18.973 ± 0.016	19.149 ± 0.030	
03/08/2009	5047.13	148.63			19.262 ± 0.027	19.430 ± 0.025	

*Observed phase with respect to the epoch of *B* maximum: JD 245 4898.5.

Table 3. Log of spectroscopic observations of SN 2009an.

Date	JD 245 0000+	Phase* (d)	Range Å
01/03/2009	4892.29	−6.21	3500-7800; 5200-9250
02/03/2009	4893.35	−5.15	3500-7800; 5200-9250
03/03/2009	4894.41	−4.09	3500-7800; 5200-9250
06/03/2009	4897.31	−1.19	3500-7800; 5200-9250
10/03/2009	4901.30	+2.80	3500-7800; 5200-9250
15/03/2009	4906.49	+7.99	3500-7800; 5200-9250
27/03/2009	4918.20	+19.70	3500-7800; 5200-9250
30/03/2009	4921.31	+22.81	3500-7800; 5200-9250
03/04/2009	4925.42	+26.92	3500-7800; 5200-9250
07/04/2009	4929.21	+30.71	3500-7800; 5200-9250
10/04/2009	4932.40	+32.90	3500-7800; 5200-9250
15/04/2009	4937.29	+38.79	3500-7800; 5200-9250
24/04/2009	4946.26	+47.76	3500-7800; 5200-9250
28/04/2009	4950.27	+51.77	3500-7800; 5200-9250
29/04/2009	4951.32	+52.82	3500-7800; 5200-9250
07/05/2009	4959.25	+60.75	3500-7800; 5200-9250
12/05/2009	4964.30	+65.80	3500-7800; 5200-9250
21/05/2009	4973.23	+74.73	3500-7800; 5200-9250
10/06/2009	4993.18	+94.68	3500-7800; 5200-9250
23/06/2009	5006.18	+107.68	3500-7800; 5200-9250

*Observed phase with respect to the epoch of *B* maximum: JD 245 4898.5.

R-bands occurs ∼2 d after the maximum in the *B*-band, whereas in the *U* and *I*-bands the maximum occurs ∼0.5 and ∼1.5 d before the *B* maximum, respectively. The tendency for the *I*-band maximum to occur before the *B*-band maximum has been observed in other SNe Ia (Anupama, Sahu & Jessy 2005; Benetti et al. 2004). The *R* and *I* light curves each show a secondary maximum, occurring ∼20 and ∼25 d after the first maximum, respectively. The secondary maxima in the *R* and *I*-bands are ∼0.82 and ∼0.38 mag fainter than the first maximum.

The absolute light curve of SN 2009an in the *R*-band has been compared with those of other well-studied SNe Ia, with different values of the decline-rate parameter $\Delta m_{15}(B)$: SN 2005hk [$\Delta m_{15}(B) = 1.68 \pm 0.05$, $E(B-V) = 0.11$, $\mu = 33.46$; Sahu et al. (2008)], SN 2004eo [$\Delta m_{15}(B) = 1.45 \pm 0.04$, $E(B-V) = 0.109$, $\mu = 34.12$; Pastorello et al. (2007)], SN 2003hv [$\Delta m_{15}(B) = 1.61 \pm 0.02$, $E(B-V) = 0.016$, $\mu = 31.37$; Leloudas et al. (2009)], SN 2003du [$\Delta m_{15}(B) = 1.04 \pm 0.04$, $E(B-V) = 0.01$, $\mu = 32.89$; Anupama et al. (2005)], SN 1991T [$\Delta m_{15}(B) = 0.95 \pm 0.05$, $E(B-V) = 0.13$, $\mu = 30.72$; Lira et al. (1998), Phillips et al. (1992)] and SN 1991bg [$\Delta m_{15}(B) = 1.93 \pm 0.08$, $E(B-V) = 0.05$, $\mu = 31.09$; Filippenko et al. (1992), Turatto et al. (1996)]. All light curves have been normalized to the epoch of *B*-band maximum for each supernova and are plotted in Fig. 3.

From Fig. 3 it is clear that in the *R*-band SN 2009an is more than 1 mag brighter than the peculiar SN 2005hk and the underluminous SN 1991bg, fainter than SNe 1991T, 2003du and 2004eo, and has a

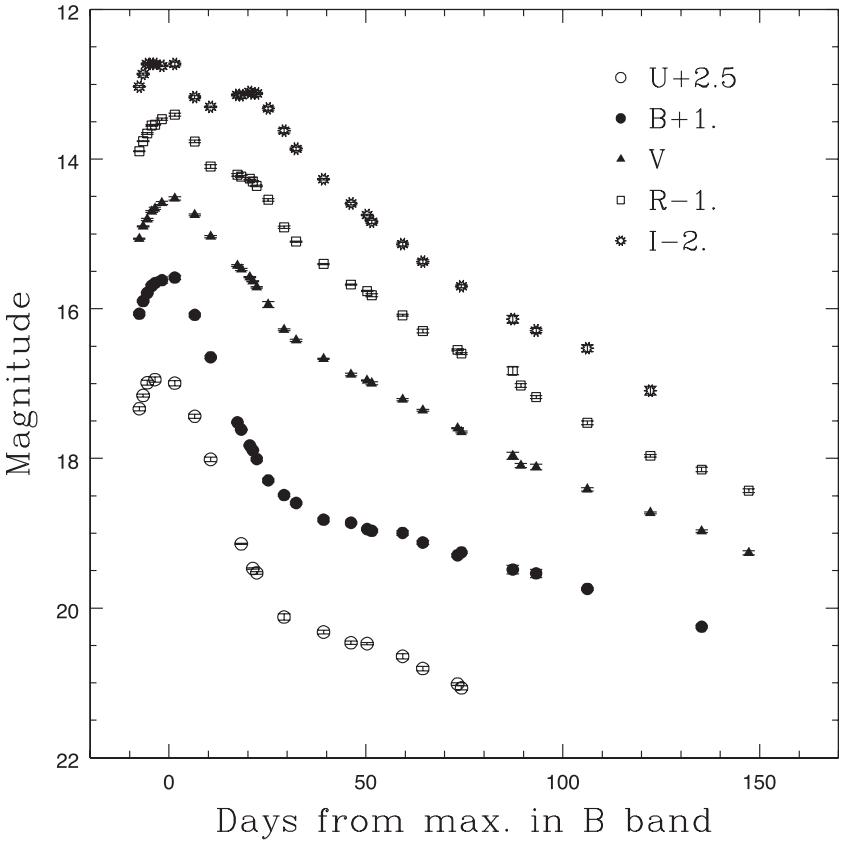

Figure 2. *UBVRI* light curves of SN 2009an. The light curves have been shifted by the amount indicated in the legend.

Table 4. Photometric parameters of SN 2009an.

Data	U	B	V	R	I
Epoch of max*	4897.9 ± 1.0	4898.5 ± 1.0	4900.9 ± 0.6	4900.4 ± 0.5	4896.1 ± 0.5
Magnitude at max	14.383 ± 0.030	14.547 ± 0.025	14.530 ± 0.013	14.429 ± 0.017	14.717 ± 0.010
Δm_{15}	1.519	1.514	0.826	0.757	0.581
Decline rate at $t > 60$ d†,+	2.70	1.589	2.320	2.775	3.00
Colours at B max		$U-B$	$B-V$	$V-R$	$R-I$
		−0.105 ± 0.043	0.065 ± 0.032	0.071 ± 0.034	−0.288 ± 0.035

*JD 245 0000+
† mag (100 d)$^{-1}$
+Days since B maximum

similar brightness to SN 2003hv. A prominent secondary maximum is seen that is absent in the light curves of the peculiar and underluminous Type Ia objects. Although in the early phase the R-band light curves of the transitional objects SNe 2009an, 2003hv and 2004eo are similar to those of SNe 1991T and 2003du, in the late phase (>60 d after B maximum) they differ considerably. The late-phase decline rate of the transitional objects is found to be faster (decline rate ∼2.45–3.04 mag/100 d) than those of SN 2003du (decline rate 1.60 mag/100 d) and SN 1991T (decline rate 1.98 mag/100 d). A similar trend is also seen in the late-phase decline rates in the B and V-band light curves. The B-band decline rate for transitional objects is 1.58–1.76 mag/100d, as compared with the ∼1.4 mag/100 d decline rate in SNe 1991T and 2003du. In the V-band, the decline rate is 2.06–2.58 mag/100 d for the transitional objects, while it is 1.70 mag/100 d for SN 1991T and 1.53 mag/100 d for SN 2003du.

The de-reddened $(U-B)$, $(B-V)$, $(V-R)$ and $(R-I)$ colour curves of SN 2009an are plotted in Fig. 4. A reddening value of $E(B-V) = 0.108$ is used (see Section 4.1). For the purpose of comparison, colour curves of SN 2003hv (Leloudas et al. 2009), SN 2003du (Anupama et al. 2005) and SN1991T (Lira et al. 1998) are also plotted in the same figure. The colours of the supernovae used here for comparison are reddening-corrected using the Cardelli, Clayton & Mathis (1989) extinction law and the $E(B-V)$ values reported earlier. The $(U-B)$, $(B-V)$, $(V-R)$ and $(R-I)$ colour evolution of SN 2009an is very similar to the colour evolution of the other normal Type Ia and SN 1991T-like objects used in comparison. The colours at the B-band maximum are tabulated in Table 4.

The transitional Type Ia supernovae 2009an, 2003hv and 2004eo are all found to be intermediate decliners, with $\Delta m_{15}(B) \sim 1.50$–1.85. They have properties that are very different from the fast-declining, underluminous SN 1991bg-like objects. The I-band

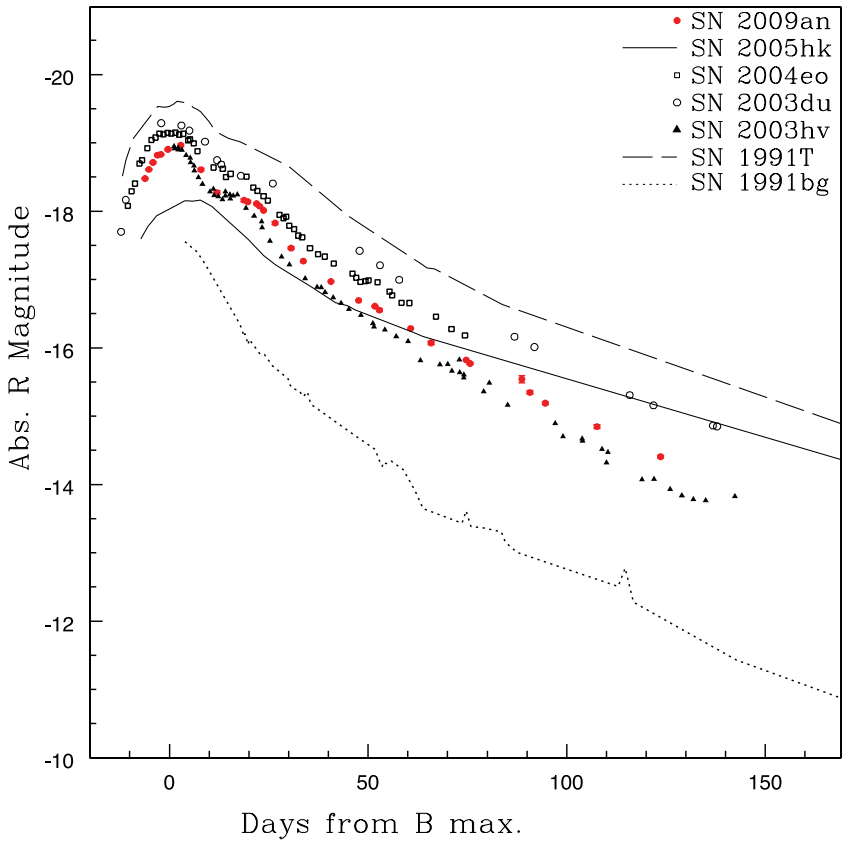

Figure 3. Absolute *R*-band light curves of SN 2009an, plotted along with those of SNe 2005hk, 2004eo, 2003du, 2003hv, 1991T and 1991bg for comparison. The reddening and distance modulus used for estimating the absolute *R* magnitude are noted in the text.

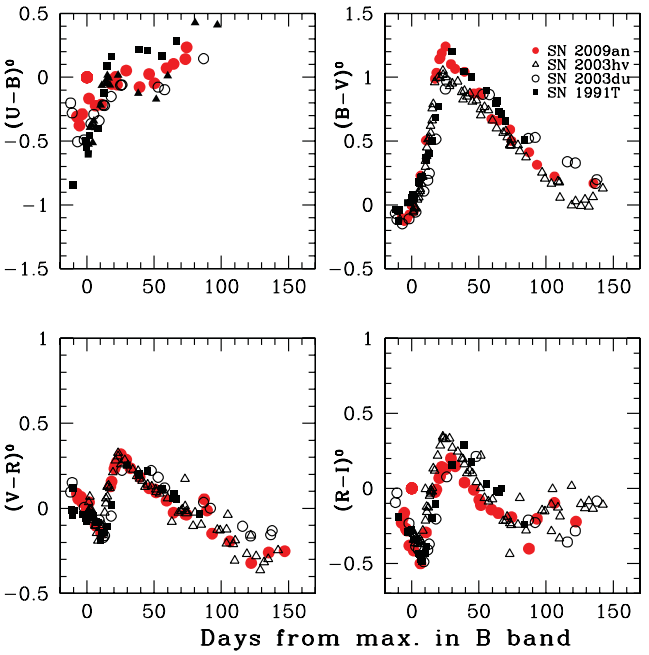

Figure 4. The $(U - B), (B - V), (V - R)$ and $(R - I)$ colour curves of SN 2009an. Also plotted are the colour curves of SNe 2003hv, 2003du and 1991T, for the purpose of comparison. The colour curves have been corrected for reddening as noted in the text.

maximum is delayed with respect to the *B*-band maximum by a few days in the case of the fast decliners. Furthermore, these objects do not show a prominent secondary maximum like that seen in the normal SNe Ia. The SN 1991bg-like events have an unusually red $(B - V)$ colour at early epochs, and they reach their reddest colour earlier than normal SNe Ia (Modjaz et al. 2001). In contrast to this, the intermediate decliners (transitional Type Ia) have double-peaked *I*-band light curves, and the first *I*-band maximum precedes that of the *B*-band by a few days, as in the case of normal SNe Ia. The colour evolution is also similar to that of normal SNe Ia. Thus, although somewhat underluminous compared with the normal SNe Ia, the transitional Type Ia events are photometrically similar to the normal SNe Ia rather than to the underluminous ones.

4 REDDENING AND DISTANCE MODULUS

4.1 Reddening estimate

The reddening experienced by a supernova can be estimated by comparing the observed broad-band colours of the supernova at different phases with the expected colours in the absence of any reddening as suggested by Lira et al. (1995), Phillips et al. (1999), Altavilla et al. (2004) and more recently by Folatelli et al. (2010). Lira et al. (1995) and Folatelli et al. (2010) used the uniform $(B - V)$ colour evolution of unreddened SNe Ia between 30 and 90 d after maximum light, whereas Altavilla et al. (2004) and Phillips et al. (1999) used colours at maximum to estimate the reddening. The total reddening estimated using the Lira et al. (1995) and Folatelli

et al. (2010) methods are $E(B-V) = 0.108 \pm 0.044$ and 0.147 ± 0.047. However, the Phillips et al. (1999) and Altavilla et al. (2004) methods, which depend on the initial decline rate of the supernova and use colour at maximum, give significantly smaller values for the total reddening, namely $E(B-V) = 0.035 \pm 0.049$ and 0.011 ± 0.08.

An independent way of estimating reddening is through the equivalent width of the Na ID lines present in the spectra of the supernova. Early-phase spectra of SN 2009an exhibit a narrow Na ID absorption line in the rest-frame of the host galaxy, with an average equivalent width $EW = 0.56 \pm 0.16$ Å. Using the relationship in Turatto, Benetti & Cappellaro (2003), we estimate $E(B-V) = 0.089 \pm 0.025$. The reddening within our Galaxy in the direction of SN 2009an is $E(B-V)_{\rm Gal} = 0.019$ (Schlegel, Finkbeiner & Davis 1998). Including the Galactic component of reddening $E(B-V)_{\rm Gal} = 0.019$, the total reddening experienced by SN 2009an is estimated to be $E(B-V)_{\rm total} = 0.108$. This value of the total reddening is in good agreement with the estimate made using the Lira relation. Hence, an $E(B-V)_{\rm total} = 0.108$ is used for extinction correction.

4.2 The absolute magnitude of SN 2009an

NGC 4332, the host galaxy of SN 2009an, has a radial velocity corrected for Local Group infall into the Virgo cluster $v_{\rm Vir} = 3029\,{\rm km\,s^{-1}}$ (LEDA). Assuming $H_0 = 72\,{\rm km\,s^{-1}\,Mpc^{-1}}$ (Freedman et al. 2001), we derive a distance $d = 42.07$ Mpc and a distance modulus $\mu = 33.12 \pm 0.15$ mag. By using the total reddening estimated as $E(B-V) = 0.108$ mag (see Section 4.1) and the Cardelli et al. (1989) extinction law, we obtain $M_U^{\rm max} = -19.26 \pm 0.20$, $M_B^{\rm max} = -19.02 \pm 0.20$, $M_V^{\rm max} = -18.93 \pm 0.20$, $M_R^{\rm max} = -18.94 \pm 0.20$ and $M_I^{\rm max} = -18.56 \pm 0.20$.

There are alternative ways to estimate the peak absolute magnitude of SNe Ia. The peak absolute magnitude of SNe Ia is known to correlate well with the initial decline-rate parameter $\Delta m_{15}(B)$. There are various calibrations available for the relation between peak absolute magnitude and $\Delta m_{15}(B)$ (Hamuy et al. 1996; Phillips et al. 1999; Altavilla et al. 2004; Reindl et al. 2005; Prieto, Rest & Suntzeff 2006). Furthermore, the intrinsic $(B-V)$ colour at 12 d after maximum light ($\Delta {\rm C}_{12}$) is correlated with the absolute magnitude (Wang et al. 2005). Phillips et al. (1999) have shown that, because of the rapid spectral evolution of SNe Ia and the small dependence of the reddening on the colour of the source, the observed $\Delta m_{15}(B)$ must be corrected for reddening. The observed value of $\Delta m_{15}(B)$ for SN 2009an translates to a reddening-corrected $\Delta m_{15}(B)_{\rm true} = 1.525$. The peak absolute magnitudes of SN 2009an in various bands using these calibrations are estimated and are reported in Table 5. Average values of the peak absolute magnitudes are also reported in the same table. These average values are consistent with the estimates made independently using the radial velocity measurement of the host galaxy. The estimated peak magnitudes show that in the *B*-band SN 2009an is fainter than normal SNe Ia by ∼0.5 mag, whereas the underluminous SN 1991bg-like objects are fainter by ∼1–2 mag than the normal Type Ia events. Furthermore, the existence of secondary maxima in the *R*- and *I*-band light curves indicates that SN 2009an is not a SN 1991bg-like underluminous object.

The time (in days) taken by a SN Ia to reach maximum light from its explosion is known as the rise time $t_{\rm r}$. The rise time is well correlated with the the peak luminosity and post-maximum decline in the sense that supernovae with brighter peak luminosities and broader light curves have longer rise times in the *B*-band. Precise knowledge of the rise time provides constraints on the models of SNe Ia (Riess et al. 1999; Fink et al. 2010). Pskovskii (1984) has shown that the rise time can be estimated using the post-maximum decline rate β (mag/100 d):

$$t_{\rm r} = 13 + 0.7\beta,$$

where β is closely related to $\Delta m_{15}(B)$. For SN 2009an, with $\Delta m_{15}(B)_{\rm true} = 1.525$, we estimate a rise time of $\sim 20.1 \pm 0.6$ d, which is marginally longer than the rise time to the *B* maximum of 19.5 ± 0.2 d for a typical SN Ia with $\Delta m_{15}(B) = 1.1$ mag and a peak $M_V = -19.45$ (Riess et al. 1999). However, owing to the lack of photometry at very early times, we did not try to estimate the rise time using the method proposed by Riess et al. (1999).

5 THE BOLOMETRIC LIGHT CURVE

The bolometric light curve of SN 2009an is estimated using the broad-band *UBVRI* magnitudes presented here. In the early phase, for missing bands, magnitudes are interpolated using the points adjacent in time. Our *U*-band observations extend up to ∼75 d after maximum light, and we have not included the contribution of the *U*-band for estimating bolometric flux beyond 75 d. During the early phase, ∼80 per cent of the bolometric flux from a SN Ia emerges in the optical region (Suntzeff 1996), and hence the integrated flux over the *U*, *B*, *V*, *R* and *I* bands gives a good estimate of the bolometric flux. The magnitudes are corrected for reddening $E(B-V) = 0.108$ (see Section 4.1) and the Cardelli et al. (1989) extinction law. The de-reddened magnitudes are then converted to monochromatic fluxes using the zero-points from Bessell, Castelli & Plez (1998). The bolometric fluxes are derived by fitting a spline curve to the *U*, *B*, *V*, *R* and *I* fluxes and integrating over the wavelength range 3100 to 10 600 Å. The bolometric luminosity is calculated using a distance of 42.07 Mpc. The bolometric light curve of SN 2009an is plotted in Fig. 5. For the purpose of comparison, the bolometric

Table 5. Peak absolute magnitude of SN 2009an obtained using the correlation between $\Delta m_{15}(B)$ and absolute magnitude, using various calibrations. All absolute magnitudes have been scaled to $H_0 = 72\,{\rm km\,s^{-1}\,Mpc^{-1}}$.

Method	$M_{B,\,\rm max}$	$M_{V,\,\rm max}$	$M_{I,\,\rm max}$
Hamuy et al. (1996)	-18.703 ± 0.102	-18.744 ± 0.094	-18.527 ± 0.082
Phillips et al. (1999)	-18.588 ± 0.181	-18.645 ± 0.160	-18.478 ± 0.124
Altavilla et al. (2004)	-18.950 ± 0.142		
Reindl et al. (2005)	-18.935 ± 0.085	-18.880 ± 0.073	-18.732 ± 0.065
Wang et al. (2005)	-18.901 ± 0.183	-18.922 ± 0.195	-18.668 ± 0.133
Prieto et al. (2006)	-18.966 ± 0.106	-18.915 ± 0.092	-18.632 ± 0.101
Average values	-18.840 ± 0.157	-18.821 ± 0.121	-18.607 ± 0.103

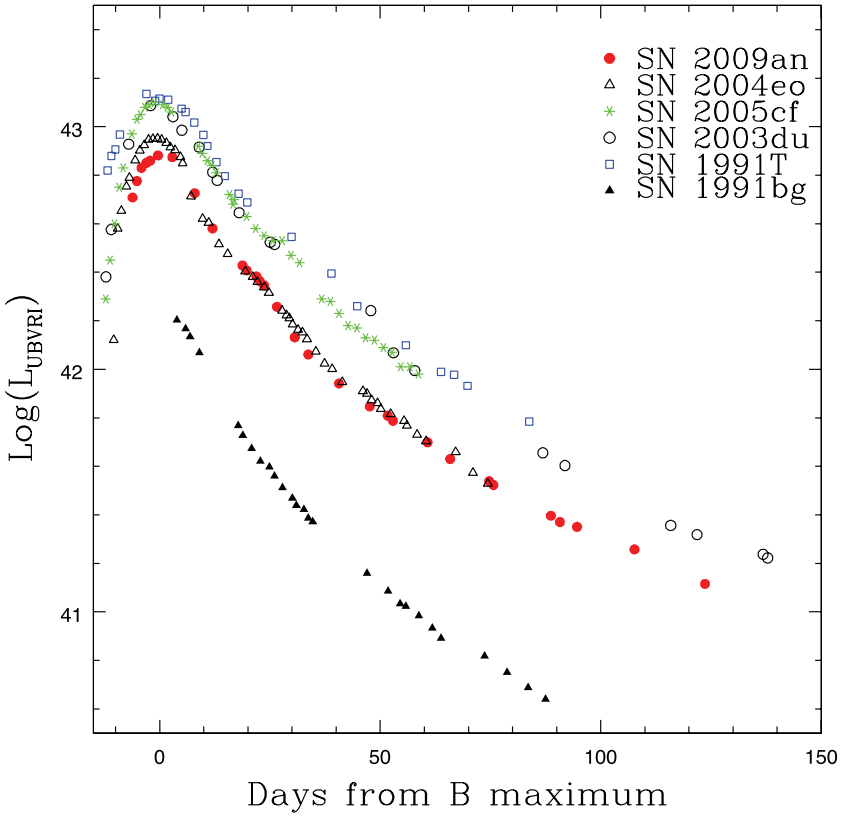

Figure 5. Bolometric light curve of SN 2009an and other well-studied SNe Ia of different subclasses.

light curves of SNe 2004eo, 2005cf, 2003du, 1991T and 1991bg are also plotted. The bolometric light curve of SN 2009an peaks at JD 245,4898.8, with a peak bolometric luminosity of $\log L_{\rm bol} = 42.89$ erg s^{-1}. Except for the marginally fainter peak, the bolometric light curve of SN 2009an is very similar to that of SN 2004eo. It is fainter than the bolometric light curves of normal/luminous Type Ia supernovae SNe 2005cf, 2003du and 1991T and brighter than SN 1991bg.

Using *HST* and *IUE* spectrophotometry for SNe 1990N and 1992A, Suntzeff (1996) estimated that the flux in the UV region drops well below 10 per cent before maximum. Contardo et al. (2000) showed that the near-infrared (NIR) passbands add at most 10 per cent at early times, and no more than about 15 per cent around 80 d after *B* maximum. Recently, Wang et al. (2009) showed that for SN 2005cf the UV contribution is generally a few per cent of the optical flux, with a peak (∼10 per cent) around the *B* maximum, and later the ratio remains at a level of 3–4 per cent. Using NIR data on SNe 2005cf, 2001el and 2004S, Wang et al. (2009) showed that the NIR to optical flux ratio shows a sharp decrease before maximum, and then it rises rapidly in a linear fashion and reaches a peak (∼20 per cent) at $t \sim 30$ d. The NIR contribution declines linearly during the nebular phase, reaching <10 per cent at ∼80 d after *B* maximum. The correction factor required to be applied to obtain the *uvoir* luminosity from *UBVRI* data alone is estimated to be around 20 per cent, with a slightly larger fraction at $t \sim 30$ d owing to the appearance of a secondary maximum in the NIR bands (Wang et al. 2009). In the case of intermediate decliners $\Delta m_{15}(B) \sim 1.50$–1.85 like SN 2004eo, the NIR *JHK* bands contribute ∼16 per cent to the total bolometric flux around maximum and ∼37 per cent one month after maximum (Pastorello et al. 2007; Taubenberger et al. 2008). Hence, adding about 20 per cent to the estimated flux to compensate for the missing bands in the UV and NIR, the peak bolometric flux is estimated to be $\log L_{\rm bol} = 42.97$ erg s^{-1}.

Another important parameter, the mass of ^{56}Ni synthesized in the explosion, can be estimated using the peak bolometric flux. Using Arnett's law (Arnett 1982) and the expression for the maximum luminosity produced by the radioactive decay of ^{56}Ni (Stritzinger & Leibundgut 2005),

$$L_{\rm max} = \left(6.45e^{-t_{\rm r}/(8.8{\rm d})} + 1.45e^{-t_{\rm r}/(111.3{\rm d})}\right) \times \left(M_{\rm Ni}/{\rm M}_{\odot}\right) \times 10^{43}\ {\rm erg\ s^{-1}},$$

where $t_{\rm r}$ is the rise time of the bolometric light curve, and $M_{\rm Ni}$ is the mass of ^{56}Ni. The estimated *B*-band rise time of SN 2009an is 20 d. Contardo et al. (2000) found the rise time of the bolometric light curve to be within one day of the rise time in the *B*-band. Using a rise time $t_{\rm r}$ of 20 d and a peak bolometric luminosity of $\log L_{\rm bol} = 42.89$ erg s^{-1}, the mass of ^{56}Ni synthesized during the explosion is estimated to be 0.41 M$_{\odot}$. If another 20 per cent of flux is added to account for the missing UV and NIR fluxes, the mass of ^{56}Ni is estimated to be 0.50 M$_{\odot}$. The other objects with an intermediate decline rate in the *B*-band light curve, for example SNe 1992A, 2003hv and 2004eo, have a mass of ^{56}Ni in the same range.

6 SPECTROSCOPIC RESULTS

6.1 Spectral evolution

The spectral evolution of SN 2009an is presented in Figs 6, 9 and 11. Fig. 6 shows the spectral evolution at the pre-maximum and around the maximum phase. The prominent lines in the pre-maximum spectrum were identified following Kirshner et al. (1993). The

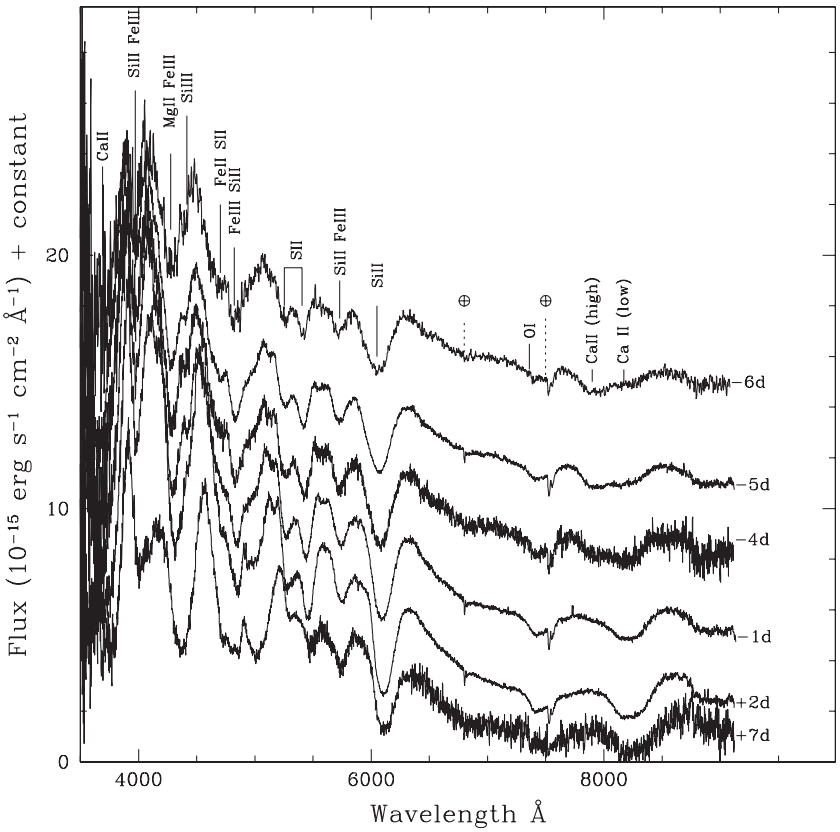

Figure 6. Spectral evolution of SN 2009an in the pre-maximm and around maximum phase (day −6 to day +7). The phases are relative to the date of *B* maximum. The spectra have been corrected for the host-galaxy redshift and reddening. For clarity, the spectra are displaced vertically. The main features are marked. The telluric lines have not been removed and are marked with the symbol ⊕.

post-maximum spectral evolution is plotted in Fig. 9, and the early nebular and nebular phase spectral evolution is shown in Fig. 11. The prominent features in the spectra were identified following Mazzali et al. (2008), who modelled the spectra of SN 2004eo.

The first spectrum, observed on JD 245 4892.29, corresponds to ∼6 days before *B* maximum. It shows a blue continuum with a well-developed Si II 6355 Å absorption, and a weaker Si II 5972 Å. Other features in the spectrum include those due to Ca II H&K, Mg II 4481 Å, possibly blended with Si III lines, and well-developed W-shaped S II lines at 5454 and 5640 Å. Blends due to Fe II, Si II and S II are also seen between 4000 and 5000 Å. The Ca II NIR triplet at 8498, 8542 and 8662 Å appears to have two components corresponding to low and high velocities. There is a hint of O I 7774 also in the first spectrum, which becomes stronger and is seen prominently until ∼+20 d. The pre-maximum and early post-maximum spectra appear similar, with some noticeable changes during this interval. The absorption strength of the Si II, S II and Ca II lines increases during this phase. The increase in the strength of the S II line is attributed to recombination, and to an increased abundance as deeper layers are exposed (Mazzali et al. 2008). The single absorption trough between 4800 and 5000 Å identified as Fe III in the −6 d spectrum splits into two troughs in the +2 d spectrum as Fe II dominates over Fe III. A change in the shape of the continuum is noticed in the spectrum of +7 d. A high-velocity feature in the Ca II NIR triplet is seen in the spectra during the interval −6 to +7 d.

In Fig. 7, spectra of SN 2009an at $t = -6$ d (top panel) and at $t = -1$ d (bottom panel) are plotted. Spectra of SN 2004eo (Pastorello et al. 2007), SN 2003du (Anupama et al. 2005), SNe 1994D and 1996X (Salvo et al. 2001) are also plotted in the same figure for comparison. All SNe show the presence of the high-velocity component in the Ca II IR triplet feature. It is also seen that the spectrum of SN 2009an is very similar to that of SN 2004eo, with comparable strength and widths of lines due to singly ionized intermediate-mass elements. In both these SNe, the Si II 6355 Å line is broad, and the Si II 5972 Å absorption is stronger than in SN 2003du. The Ca II H&K lines show a single, flat-bottomed profile, while in SN 1994D it is split into two. The line profile around 4500 Å is also found to be different. While SN 2009an (and SN 2004eo) shows a single deep absorption, the other SNe Ia, such as SNe 1994D and 1996X, show two absorption troughs, which are identified as due to Mg II 4481 Å and Si III 4553, 4568 Å, with almost equal strength. We identify the absorption in SN 2009an to be due to Mg II, with Si III being weak or absent. The strength of the Si III line is found to be correlated with temperature (Pignata et al. 2008). This indicates that SN 2009an has a lower photospheric temperature than SNe 1994D or 1996X.

We use the parametrized spectrum synthesis code 'SYN++' to identify various species in the observed spectrum and to derive other physical parameters. 'SYN++' is a rewrite of the original SYNOW code (refer to https://c3.lbl.gov/es/ for further details of SYN++) with a new structured input control file format and more complete atomic data files. The SYNOW code assumes a spherically symmetric and homologously expanding ejecta ($v \propto r$) and resonant scattering line formation above a sharp photosphere emitting a blackbody continuum. The line formation is treated using the Sobolev approximation (Sobolev 1957; Jeffery & Branch 1990). The optical depth τ of the strongest line is a free-fitting parameter, and the optical depths of

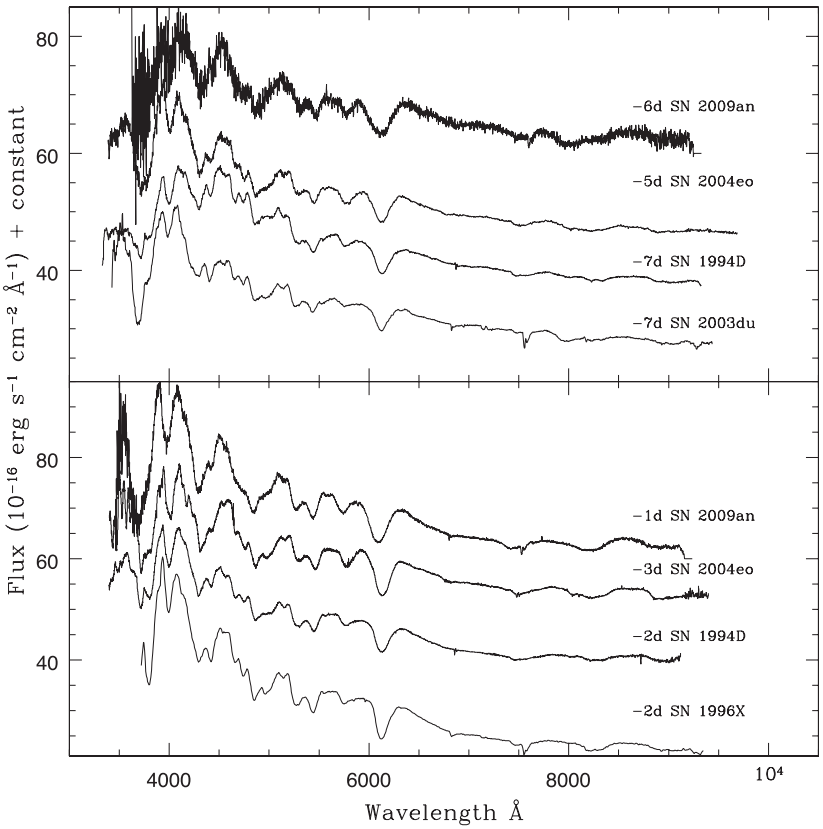

Figure 7. Pre-maximum spectrum of SN 2009an compared with those of Type Ia SNe 2004eo, 1994D, 2003du and 1996X at a similar epoch. The phases marked are relative to the date of the *B* maximum. The spectra have been corrected for the host galaxy redshift and reddening. For clarity the spectra are shifted vertically.

the other lines of the same ion are determined assuming Boltzmann equilibrium at excitation temperature $T_{\rm exc}$. A detailed description of the SYNOW code can be found in (Fisher 2000) and (Branch et al. 2002)).

The −5, −1, +8 and +31 d spectra of SN 2009an have been modelled with the SYN++ code. The early phase observed and synthetic spectra are plotted in Fig. 8. The −5 d spectrum of SN 2009an fits well with a synthetic spectrum with a blackbody temperature of 14 800 K and a photospheric velocity $v_{\rm phot}$ of 11 500 km s^{-1}. It contains lines of O I, Mg II, Si II, Si III, S II and Fe III with a photospheric velocity component only, while Ca II has both photospheric and high-velocity components (Fig. 8, top panel). The absorptions near 4000 and 4300 Å and the sawtooth-like line profile at 5000 Å can be reproduced only by introducing a Fe III line at lower velocity. Furthermore, the absorption at 5700 Å cannot be reproduced by only Si II, and introducing Fe III improves this fit also. The presence of Fe III and Si III lines in the −5 d spectrum also indicates a high temperature in the ejecta. The overall shapes of the −1 d spectrum and the −5 d spectrum are very similar, and the observed spectrum of −1 d (Fig. 8, middle panel) can be reproduced with the same species as used in the −5 d spectrum, with a marginally lower blackbody temperature (∼14 300 K) and a lower velocity for the high-velocity component of Ca II. The +8 d spectrum of SN 2009an indicates an evolution towards lower temperature and lower photospheric velocity. The observed spectrum matches well with a synthetic spectrum with a blackbody temperature of 11 500 K and a photospheric velocity $v_{\rm phot}$ of 6500 km s^{-1} (Fig. 8, bottom panel). At 5900 Å, the absorption feature is well reproduced by Si II, Fe III and Na I, indicating the emergence of Na I. In the underluminous events, the introduction of Ti II improves the fit near 4200 Å. However, in the case of SN 2009an, the introduction of Ti II does not improve the fit, implying the absence of Ti II.

The spectral evolution during +20 to +53 d is shown in Fig. 9 (top panel). During this interval, the Si II line at 5972 Å is replaced by the Na I line, which starts becoming stronger and contaminating the features near 5900 Å. Mazzali et al. (2008) identified the broad features between 4500 and 5000 Å with Fe II, probably with some contribution from Ti II, as is seen in the underluminous SN 1991bg-like events. The synthetic spectrum generated for day +31 is displayed along with the observed spectrum in Fig. 9 (bottom panel). The synthetic spectrum has a blackbody temperature of 7000 K and a photospheric velocity $v_{\rm phot}$ of 6000 km s^{-1}. During this phase, the absorption core at ∼6100 Å is reproduced by the Si II feature, and the strengthening of the Fe II features in the adjacent region make the absorption broader. The strong absorption at ∼5900 Å is reproduced mainly by Na I. The post-maximum spectra of SN 2009an are similar to those of other SNe Ia, as seen from Fig. 10.

The early nebular and nebular spectra obtained during days +61 to +107, shown in Fig. 11, indicate that the spectrum is dominated by forbidden lines of singly and doubly ionized Co and Fe by day +61. Not much evolution is seen in the spectrum during this phase. A comparison of the nebular spectra of SN 2009an with those of other SNe Ia (Fig. 12) indicates an overall similarity in all supernovae.

The overall spectral evolution of SN 2009an is very similar to that of SN 2004eo, which was shown by Pastorello et al. (2007) to be similar to that of SN 1992A, although with a lower velocity.

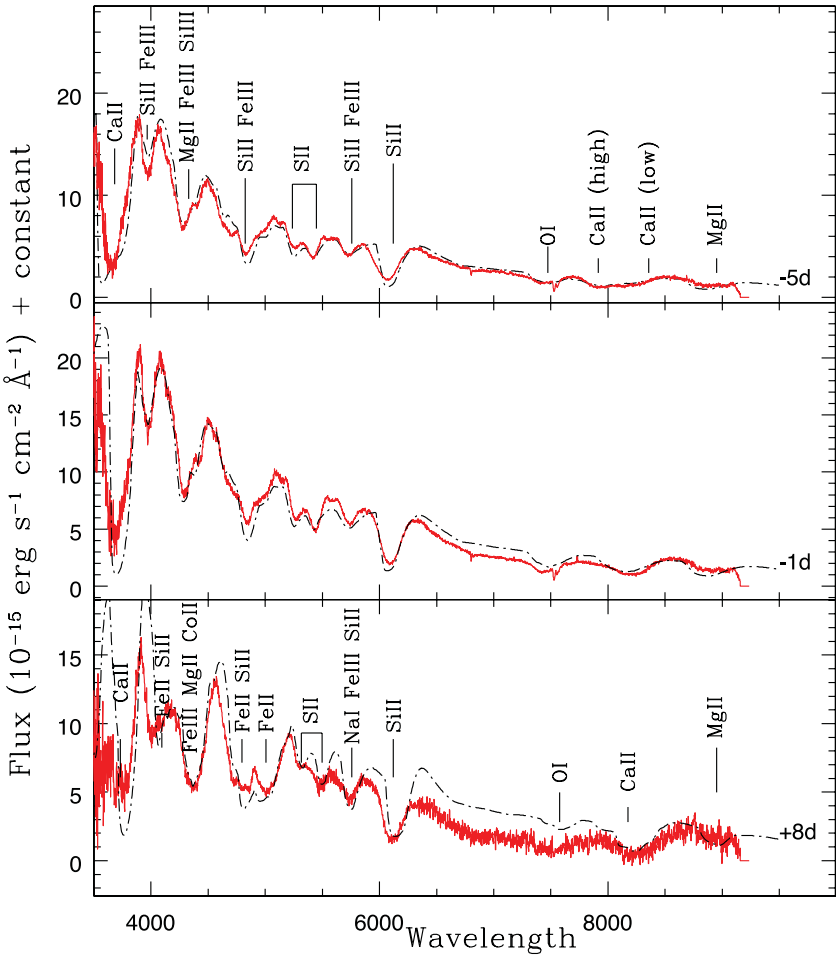

Figure 8. Observed spectra of SN 2009an (red) at −5 d (top panel), −1 d (middle panel) and +8 d (bottom panel). The observed spectra are plotted with the synthetic spectra (black) obtained with SYN++.

6.2 Expansion velocity of the ejecta

The expansion velocity of the ejecta was measured by fitting a Gaussian to the absorption trough of Ca II H&K, S II 5640 Å, Si II 6355 Å and the Ca II NIR triplet. The velocity evolution of various species is plotted in Fig. 13. We confirm the presence of a high-velocity component in the Ca II NIR triplet during the pre-maximum and early post-maximum phase, noted by Yamanaka & Arai (2009) and Vinko et al. (2009) in the spectrum of 2009 March 1. Expansion velocity estimates for both the high- and the low-velocity components are plotted in Fig. 13. Mazzali et al. (2005) have shown that almost all SNe Ia with early spectra show a high-velocity feature in the Ca II NIR triplet, but with varying strength and duration. They may be interpreted as being caused either by the enhancement in the abundance of Ca in the outer region, or by density enhancements as a result of the sweeping up of the interstellar material by the highest-velocity supernova ejecta (Mazzali et al. 2005). Gerardy et al. (2004) interpret the presence of the high-velocity feature as an indication of interaction between the circumstellar material and the supernova ejecta.

Based on the Si II velocity gradient between the time of maximum and either the time the Si II feature disappears or the last available spectrum, whichever is earlier, Benetti et al. (2005) arranged SNe Ia into three classes: (i) the FAINT class consisting of faint objects with a high velocity gradient and high Si II line ratio; (ii) the HVG class consisting of normal SNe Ia with a high velocity gradient (>70 km s^{-1} d^{-1}) and low Si II line ratio; and (iii) the LVG class with a low velocity gradient (<60–70 km s^{-1} d^{-1}). This class includes both normal and bright SNe Ia. In the case of SN 2009an, the velocity gradient of the Si II λ 6355 Å line during the interval ∼+3 to +39 d is estimated to be 60 km s^{-1} d^{-1}, which is just at the upper limit of the LVG class, similar to SNe 2004eo, 1992A and 1989B. However, Benetti et al. (2005) have also noted that for SNe 1989B and 1992A the classification is uncertain. A small variation of the parameters, still within the errors, could shift them from the LVG group to the HVG group, and the same holds for SN 2009an.

Recently, Blondin et al. (2012) suggested that instead of estimating the velocity gradient from a least-squares fit of the measurements taken between maximum and either the time the Si II feature disappears or the last available spectrum, the mean velocity decline rate should be measured over some fixed time interval. For SN 2009an, if the measured velocities at −1.19 and +7.99 d are used, a velocity decline rate of ∼93 km s^{-1} d^{-1} is estimated, shifting SN 2009an from the LVG to the HVG group.

The expansion velocity estimated using the Si II 6355 Å line is plotted in Fig. 14, with other objects belonging to the LVG and HVG groups and objects with faster-declining light curves. In the pre-maximum phase, SN 2009an has a higher expansion velocity than other objects with similar Δm_{15}(B). After the maximum, however, the expansion velocity is similar to that of SN 1992A. There are

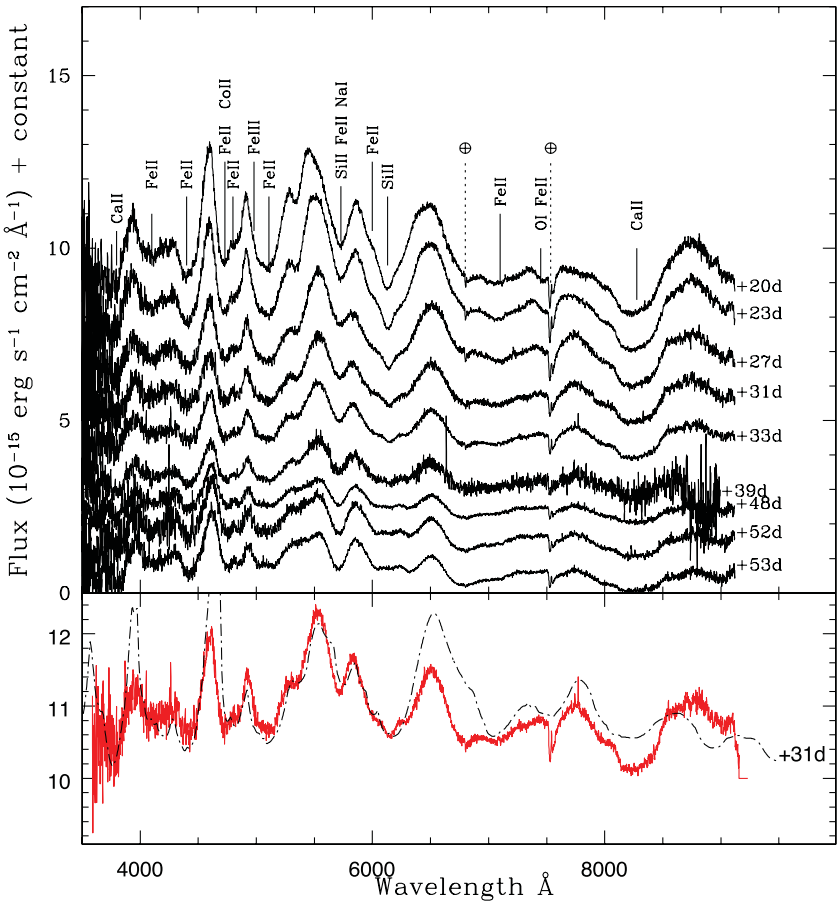

Figure 9. Top panel: Spectral evolution of SN 2009an during +20 to +53 d relative to the date of *B* maximum. The spectra have been corrected for the host-galaxy redshift and reddening. For clarity the spectra are displaced vertically. The telluric lines have not been removed and are marked with the symbol ⊕. Bottom panel: +31-d spectrum of SN 2009an (red) compared with a synthetic spectrum obtained using SYN++ (black).

some LVG supernovae that show a high expansion velocity in the pre-maximum phase, but a few days after maximum the difference in the expansion velocity among different class is not significant.

It has been suggested that the difference in the velocity gradient for the HVG and LVG classes can come either from the nature of the explosion or from the different degrees of mixing of heavy elements. One possibility suggested by Benetti et al. (2005) is that the supernovae belonging to the HVG group are the result of delayed detonation, while the explosion mechanism for the LVG group objects is deflagration. The high velocity gradient in the HVG class could arise from the efficient mixing of heavy elements to the outer ejecta, whereas less efficient mixing could be the reason for the low velocity gradient of the LVG group. In a recent theoretical study, Maeda et al. (2010) showed that a white dwarf initially ignited slightly away from the centre results in an asymmetric explosion. They suggest that the HVG and LVG supernovae do not have intrinsic differences, but that the observed diversity could be an effect of the viewing angle of such an asymmetric explosion. The supernovae that are viewed from the direction of the off-centre ignition appear as LVG events, while those viewed from the opposite direction appear as HVG events.

6.3 *R*(Si II) ratio

The ratio *R*(Si II) of the depths of two Si II lines at 5972 and 6355 Å, as defined by Nugent et al. (1995), is known to be correlated with the absolute magnitude of SNe Ia. At the *B*-band maximum, the ratio is found to be large for dimmer objects and smaller for brighter objects, and hence it could be used as a distance-independent spectroscopic luminosity indicator.

The *R*(Si II) ratio for SN 2009an is calculated using the method prescribed by Nugent et al. (1995) during the pre-maximum and early post-maximum phase. The temporal evolution of the *R*(Si II) ratio for SN 2009an along with that for other supernovae are plotted in Fig. 15. With an average pre-maximum value of 0.42 ± 0.03, no significant temporal evolution of the *R*(Si II) ratio is seen in the case of SN 2009an. Benetti et al. (2005) noted that in the pre-maximum phase, HVG SNe Ia show significant temporal evolution, starting from a high value well before maximum and levelling out just before maximum, whereas the *R*(Si II) ratio for the LVG SNe Ia stays nearly constant. Around maximum, the *R*(Si II) ratios of HVG and LVG supernovae are comparable. In Fig. 15, it is clearly seen that, in terms of the *R*(Si II) ratio, SNe 1989B, 1992A, 2004eo and 2009an are different from all other supernovae; in fact, they lie between the normal SNe Ia and the underluminous 1991bg-like events. Similar to the LVG group supernovae, the *R*(Si II) ratios for SNe 1989B, 1992A, 2004eo and 2009an do not show significant temporal evolution.

The correlation between the *R*(Si II) ratio and the luminosity of SNe Ia was interpreted as resulting from the temperature difference, which is directly related to the variation in the mass of ^{56}Ni produced in the explosion. At lower effective temperatures, a

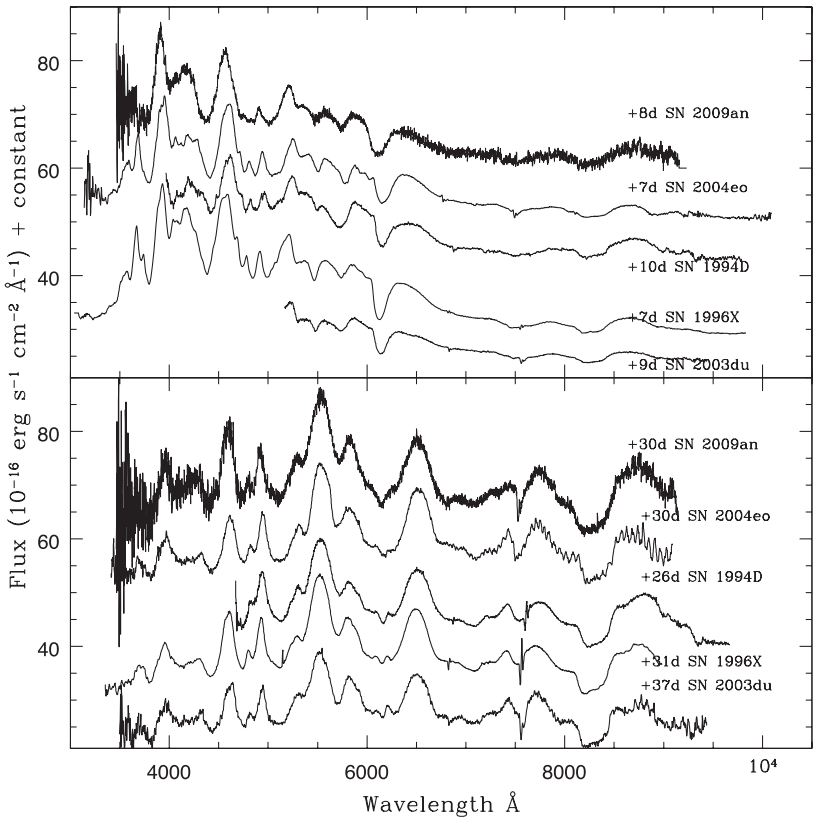

Figure 10. Comparison of the post-maximum spectrum of SN 2009an with those of Type Ia SNe 2004eo, 2003du, 1996X and 1994D, at similar epochs with respect to the date of *B* maximum. The spectra have been corrected for the host-galaxy redshift and reddening. For clarity the spectra are shifted vertically.

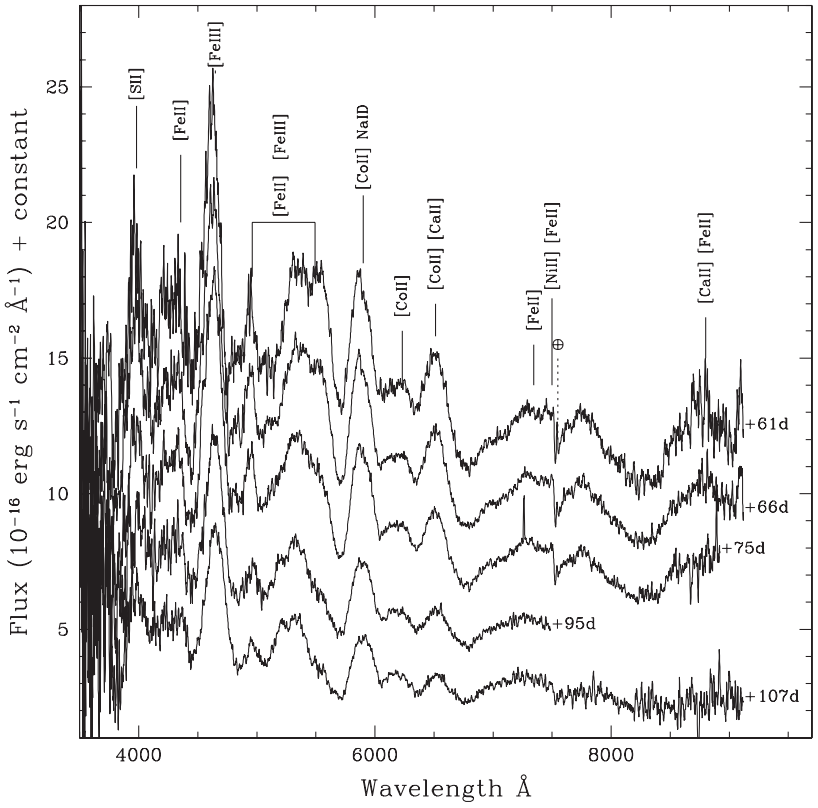

Figure 11. Spectral evolution of SN 2009an during +61 to +107 d relative to the date of *B* maximum. The spectra have been corrected for the host-galaxy redshift and reddening. For clarity the spectra are displaced vertically. The telluric lines have not been removed and are marked with the symbol ⊕.

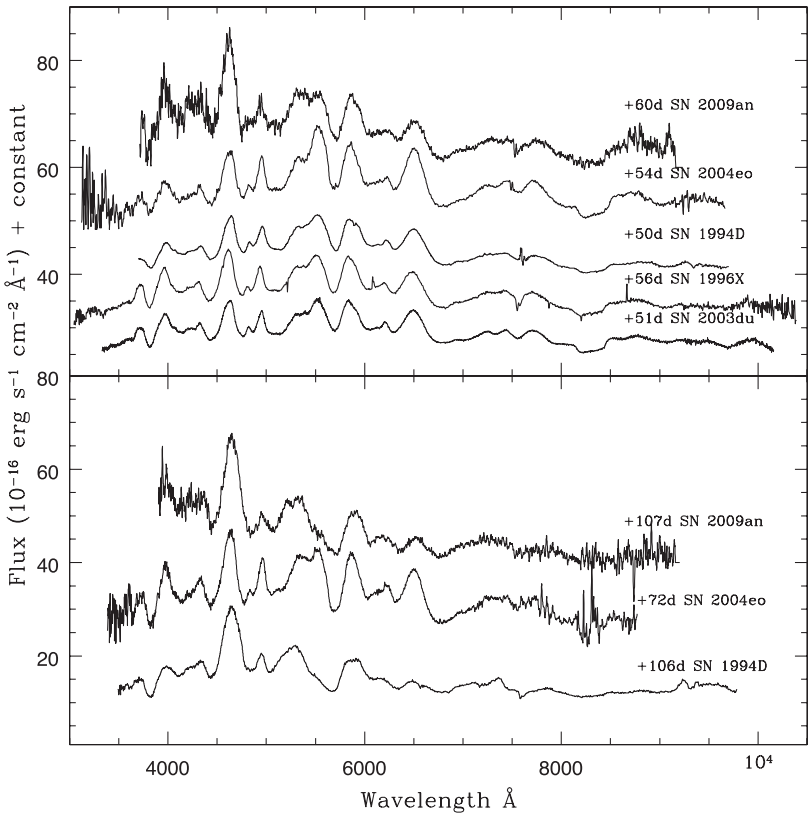

Figure 12. Late-phase spectrum of SN 2009an during ∼+60 to ∼+107 d compared with those of Type Ia SNe 2004eo, 2003du, 1996X and 1994D at a similar epoch relative to *B* maximum. The spectra have been corrected for the host galaxy redshift and reddening. For clarity the spectra are shifted vertically.

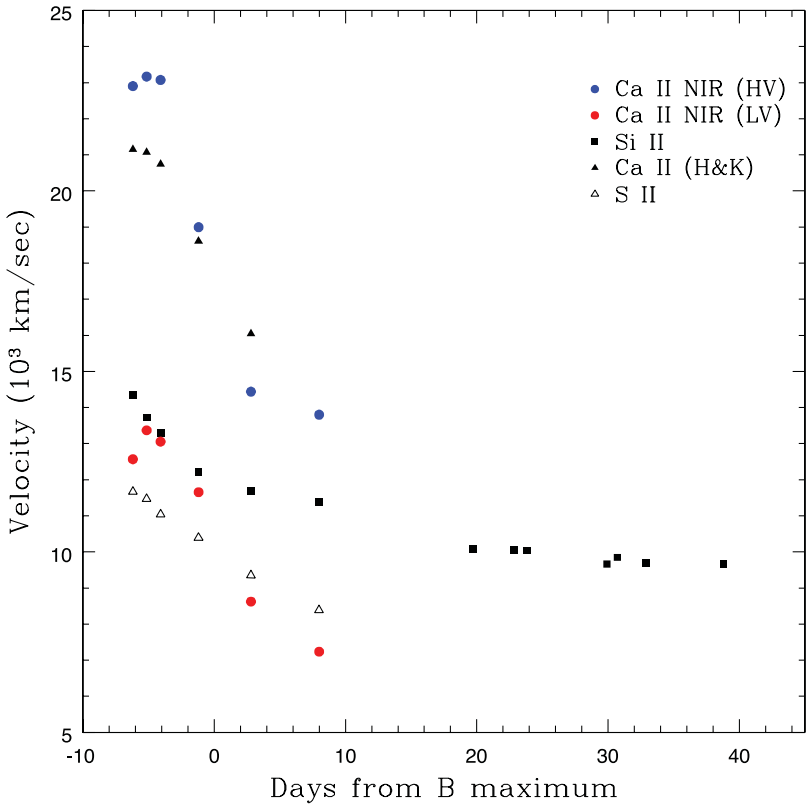

Figure 13. Velocity evolution of SN 2009an derived using the Si II λ 6355 Å Ca II H&K, Ca II NIR and S II λ 5640 Å lines.

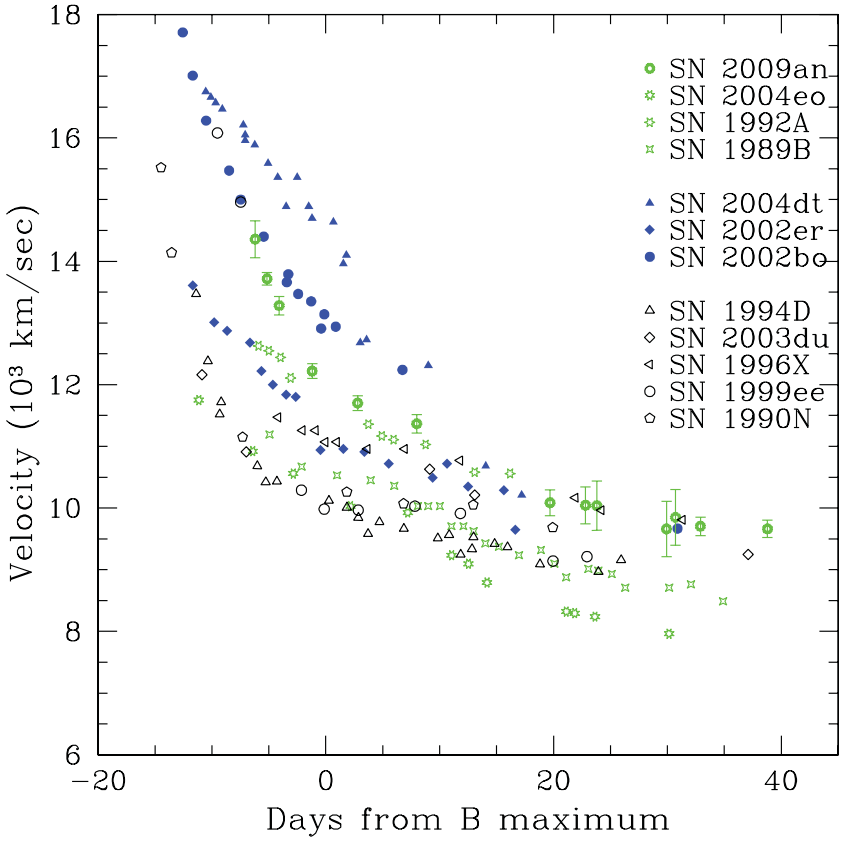

Figure 14. Velocity evolution of SN 2009an derived using the Si II λ 6355 Å line. The evolutions for other supernovae are also plotted for comparison. Objects belonging to the HVG class are represented by filled symbols, the transitional Type Ia objects are marked as open starred symbols, and open symbols represent the LVG objects.

complex interaction of the lines with line blanketing from Fe II and Co II increases the apparent strength of the 5800 Å line, and at higher effective temperatures Fe III and Co III line blanketing helps to wash out the feature at 5800 Å (Nugent et al. 1995). However, Hachinger et al. (2008) have shown that the increase of the R(Si II) ratio for luminous to dim object is caused by the increasing strength of the Si II 5972 Å line for dim objects. In less luminous objects, Si II 5972 Å is stronger because of a rapidly increasing Si II/Si III ratio. Because of its large optical depth, the Si II 6355 Å line is saturated and has a fairly constant strength. These authors also suggested that as the Si II 6355 Å line is saturated, the Si II 5972 Å line may be the best spectroscopic luminosity indicator for SNe Ia.

Branch, Dang & Baron (2006) and Branch et al. (2009) arranged the maximum light spectra of SNe Ia on the basis of measurements of W(5750) and W(6100), the (pseudo) equivalent widths of absorption features near 5750 Å (usually attributed to Si II λ5972) and 6100 Å (due to Si II λ6355) and the appearance of 6100 Å absorption. They classified the spectra of SNe Ia into four groups – core-normal, broad-line, cool, and shallow-silicon. The core-normal supernovae have very similar spectra at maximum light and post-maximum epochs, except for the varying strength of high-velocity Ca II features. The broad-line supernovae have 6100 Å absorption broader and deeper than that of core-normal supernovae. Cool supernovae have a conspicuous absorption trough at ∼4000–4500 Å due to Ti II, whereas those in the shallow-silicon group have smaller values of W(5750) and W(6100). As per the original classification by Branch et al. (2009), SN 1992A was classified as a cool supernova, SN 1989B was classified as marginal cool, with no identifiable Ti II lines, and SN 2004eo was classified as mild cool. In Section 6.1, it is shown that the synthetic spectra of SN 2009an calculated using the SYN++ code do not need the presence of Ti II.

The pseudo-equivalent widths W(5750) and W(6100), for a subset of data used by Branch et al. (2009), after including SNe 2003hv and 2009an, are plotted in Fig. 16. The five objects SNe 1989B, 1992A, 2003hv, 2004eo and 2009an, termed transitional objects, form an easily identifiable group that nicely fills the gap between the cool and core-normal supernovae. It indicates a gradual transition of properties from the cool supernovae to the core-normal supernovae, and thus the possible presence of a continuous distribution of properties amongst SNe Ia of different subclasses. In fact, using a sample that includes objects with a wider range of $\Delta m_{15}(B)$ between ∼0.7 and ∼2 mag, Blondin et al. (2012) have shown that there are no strict boundaries between the different subclasses and that there is a continuum of properties between them.

In Fig. 17, similar to fig 3(a) of Benetti et al. (2005), the value of the R(Si II) ratio at maximum light for a subsample of Branch et al. (2009), including the transitional events, is plotted against $\Delta m_{15}(B)$. In fig. 3(a) of Benetti et al. (2005) there is a gap between the group containing faint objects and the group containing HVG and LVG objects. Pastorello et al. (2007) have shown that SN 2004eo and other non-standard objects, for example SNe 1989B and 1992A, lie roughly in the middle of the diagram, between the faint group and the HVG/LVG group. In Fig. 17 we have used the nomenclature in Branch et al. (2009). It is clear from the figure that the transitional objects are located between the cool and core-normal objects, connecting the faint and normal bright Type Ia objects. Following

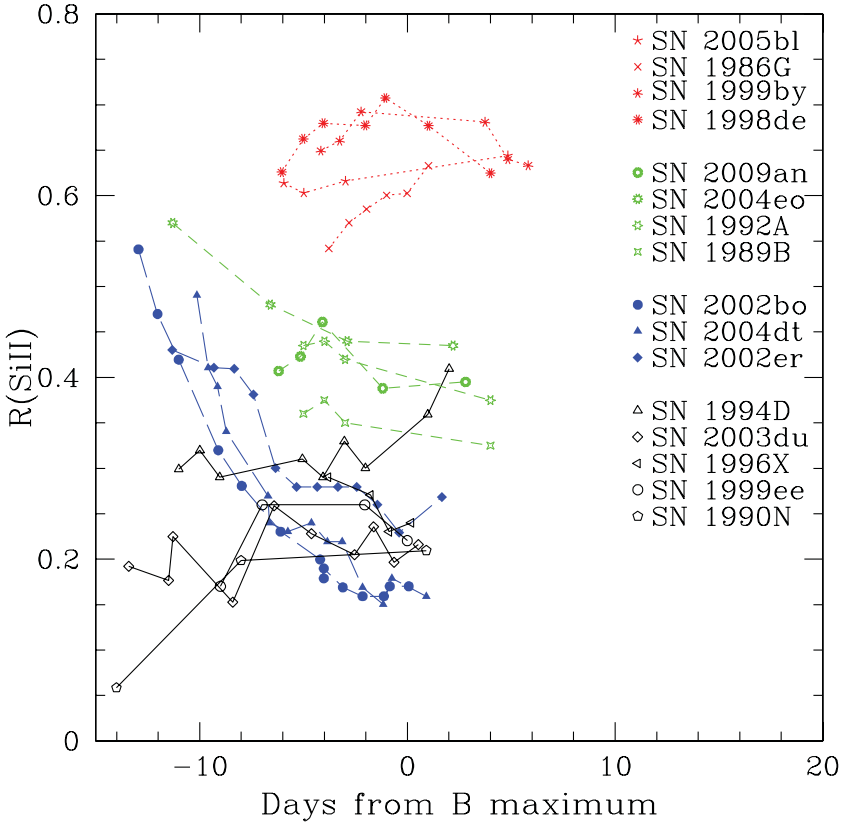

Figure 15. Temporal evolution of the R(Si II) ratio of SN 2009an, together with those of other supernovae for comparison. The SN 1991bg-like underluminous supernovae are marked as skeletal (centre connected to vertices) symbols, transitional-type events are marked as open starred symbols, filled symbols represent the HVG supernovae, and open symbols represent the LVG supernovae.

the criterion suggested by Benetti et al. (2005), the transitional objects fall in the LVG group, so it will be appropriate to consider the transitional objects as a link between the faint and the LVG SNe Ia.

7 SUMMARY

We have presented *UBVRI* photometric observations of SN 2009an during the interval ∼−6 to ∼+150 d with respect to the *B*-band maximum. The light-curve evolution of SN 2009an shows that the supernova reached its *B*-band maximum on JD 245 4898.5 ± 1 at 14.547 ± 0.025 mag. The light curves of SN 2009an declines faster than the normal SNe Ia, with a *B*-band decline rate parameter $\Delta m_{15}(B)$ of 1.514 ± 0.132. The moderately higher value of $\Delta m_{15}(B)$ for SN 2009an puts it along with SNe 2004eo and 1992A in the transitional class, between the 'normal' and 'low-luminosity SN 1991bg-like objects'. The peak absolute magnitude of SN 2009an is estimated using empirical relations. With an absolute *B*-band magnitude at peak $M_{B,\,\mathrm{max}} = -18.841 \pm 0.157$, SN 2009an is found to be dimmer than the normal Type Ia objects. The *UBVRI* bolometric luminosity of SN 2009an is derived, and the peak bolometric luminosity $\log L_{\mathrm{bol}}$ is estimated as 42.89 erg s^{-1}; this implies that 0.41 $M_\odot$ of ^{56}Ni was synthesized in the explosion. However, if another 20 per cent flux is added to account for the missing UV and NIR bands, the mass of ^{56}Ni is estimated to be 0.50 $M_\odot$, which is very close to the mass of ^{56}Ni synthesized in the explosions of other events belonging to the transitional class.

The spectroscopic data during ∼−6 to ∼+107 d are also presented. The pre-maximum spectral evolution of SN 2009an is very similar to that of the transitional-type object SN 2004eo. High-velocity features are seen in the Ca II NIR triplet during the pre-maximum and early post-maximum phase. In the pre-maximum and early post-maximum spectra, SN 2009an has a broad Si II 6355 Å line, and Si II 5972 Å is stronger than for normal Type Ia events. The post-maximum spectral evolution is similar to those of normal Type Ia objects. Based on the Si II 6355 Å line velocity gradient of 60 km s^{-1} d^{-1} during +3 to +39 d, SN 2009an is just at the upper limit of the LVG class. However, if the revised definition of the velocity decline rate is used, SN 2009an falls in the HVG class. The R(Si II) ratio does not show any significant evolution and its average value is 0.42 ± 0.03, which is between that for normal Type Ia and underluminous SN 1991bg-like events.

A study of the properties of all the known transitional Type Ia events indicates that their photometric properties ($\Delta m_{15}(B)$, M_B) and their spectroscopic luminosity indicator R(Si II) ratio lie between those of normal Type Ia objects and the underluminous SN 1991bg-like objects. In the W(5750) versus W(6100) and R(Si II) versus Δm_{15}(B) plots, the transitional objects occupy the space between underluminous 1991bg-like objects and the normal Type Ia events.

To explore whether these transitional SNe Ia bridge the gap between the normal Type Ia events and the low-luminosity SN 1991bg-like events, it is desirable to have a detailed model for these objects. The light curve and spectra of SN 2004eo have been modelled by Mazzali et al. (2008). These authors have shown that the spectral evolution, bolometric light curve and low ^{56}Ni mass of SN 2004eo can be reproduced by explosion of a Chandrasekhar-mass CO white dwarf with a lower kinetic energy (1.1 ± 0.1 × 10^{51} erg) than the W7 model kinetic energy (1.3 × 10^{51} erg), and a larger amount of

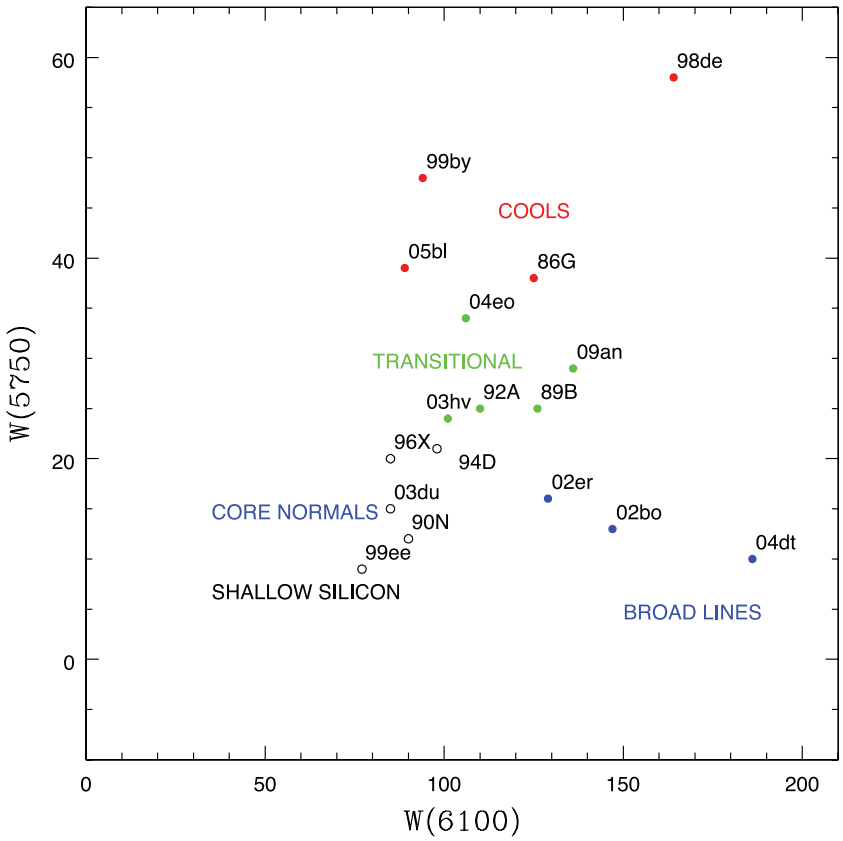

Figure 16. Plot of the pseudo-equivalent width of Si II 5972 line, $W(5750)$, versus the pseudo-equivalent width of Si II 6355 line, $W(6100)$, for a subsample of SNe Ia. The nomenclature is as in Branch et al. (2009).

stable Fe-group material. Mazzali et al. (2008) also indicated that such low-luminosity explosions may be the result of a strong initial deflagration phase, during which the star expands, and, when a delayed detonation occurs, it burns the material at low density, mostly to the intermediate mass element, which is expected to be unburned oxygen, as signature of unburned carbon is not seen in the spectra. The absence of carbon and the presence of absorption due to oxygen in the pre-maximum and early post-maximum spectra of SN 2009an are consistent with the explosion model proposed for SN 2004eo. The observed similarity between SN 2004eo and SN 2009an in terms of their photometric and spectroscopic properties may indicate that these events are the results of identical explosions, with lower kinetic energy than in the W7 model.

Even with a limited number of the transitional objects studied in detail, it appears that they fill the gap between the underluminous and the normal Type Ia events. The observed dissimilarity between the transitional and normal Type Ia events may also be influenced by the host galaxy properties. Curiously enough, the host galaxies of the known transitional objects are all group members. They are either lenticulars or spirals, and the SN is located away from the nucleus (which could be just an observational bias). We do not, however, have any information about the host galaxy metallicity, in particular at the SN location. To understand these events better, and to examine whether the transitional objects really bridge the gap between the normal Type Ia events and low-luminosity SN 1991bg-like objects, it is necessary to have a detailed study, including the robust modelling, of as many objects as possible belonging to this class. Upcoming surveys may discover more such objects, and, with a sufficiently large sample, the properties of this class of objects can be better understood.

Finally, we try to check whether the inclusion of transitional objects has any effect on cosmology. The peak absolute magnitude of the transitional objects, estimated using the extinction-corrected observed magnitude and the distance modulus, was used to estimate $\Delta m_{15}(B)$, with the help of empirical relations between absolute magnitude and $\Delta m_{15}(B)$. It is found that the empirical relations reproduce the observed $\Delta m_{15}(B)$ well, implying that their inclusion may not affect the results of SN cosmology.

ACKNOWLEDGMENTS

We would like to thank the anonymous referee, whose comments helped to improve the work considerably. We would like to express our sincere thanks to Gaston Folatelli for discussion on SYN++ fitting. We thank all the observers at the 2-m HCT who kindly provided some of their observing time for the supernova observations, and Ms Sonam Arora for help with observations. This work has made use of the NASA Astrophysics Data System and the NASA/IPAC Extragalactic Data base (NED), which is operated by the Jet Propulsion Laboratory, California Institute of Technology, under contract with the National Aeronautics and Space Administration. IRAF is distributed by the National Optical Astronomy Observatories, which are operated by the Association of Universities for Research in Astronomy, Inc., under contract to the National Science Foundation.

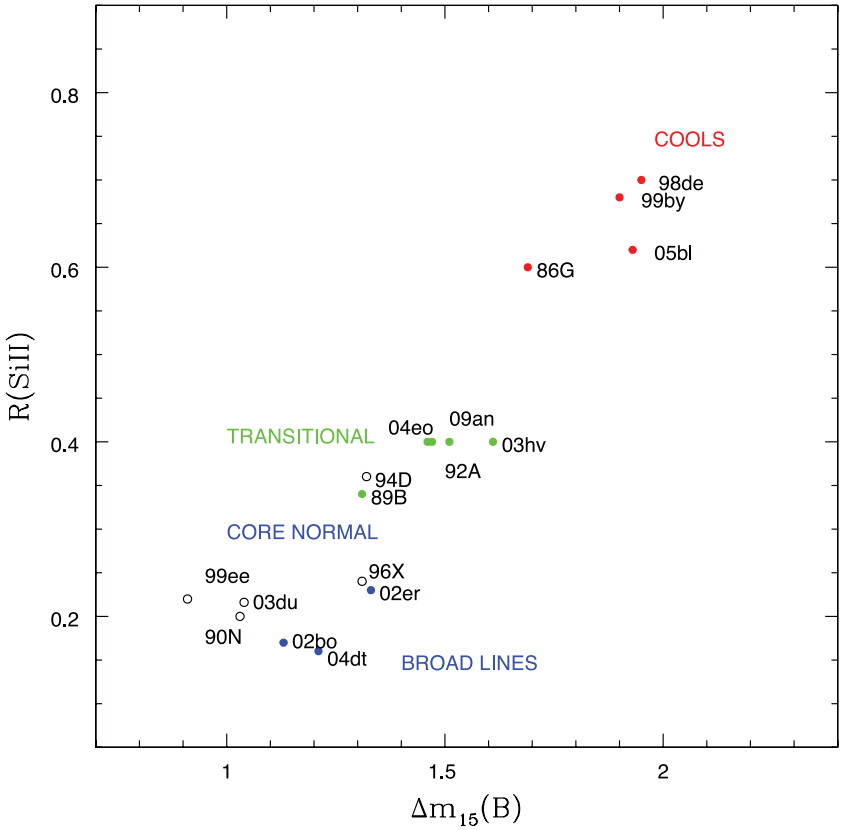

Figure 17. Plot of the R(Si II) ratio versus Δm_{15} for a subsample of SNe Ia used in Figs 15 and 16. The nomenclature is as in Branch et al. (2009).

REFERENCES

Altavilla G. et al., 2004, MNRAS, 349, 1344
Anupama G. C., Sahu D. K., Jessy J., 2005, A&A, 429, 667
Arnett W. D., 1982, ApJ, 253, 785
Benetti S. et al., 2004, MNRAS, 348, 261
Benetti S. et al., 2005, ApJ, 623, 1011
Bessell M. S., Castelli F., Plez B., 1998, A&A, 333, 231
Blondin S. et al., 2012, AJ, 143, 126
Branch D., Benetti S., Kasen D., Baron E., Jeffery D. J., Hatano K., 2002, ApJ, 566, 1005
Branch D. et al., 2006, PASP, 118, 560
Branch D., Dang L. C., Baron E., 2009, PASP, 121, 238
Bronder T. J. et al., 2008, A&A, 477, 717
Cardelli J. A., Clayton G. C., Mathis J. S., 1989, ApJ, 345, 245
Challis P., 2009, CBET, 1709, 1
Contardo G., Leibundgut B., Vecca W. D., 2000, A&A, 359, 876
Cortitini G., Antonellini S., 2009, CBET, 1707, 1
Filippenko A. V. et al., 1992, AJ, 104, 1543
Fink M., Ropke F. K., Hillebrandt W., Seitenzahl I. R., Sim S. A., Kromer M., 2010, A&A, 514, 53
Fisher A., 2000, PhD thesis, Univ. Oklahoma
Folatelli G., Phillips M. M., Burns C., Contreras C., Hamuy M., Freedman W. L., Persson S. E., Stritzinger M., 2010, AJ, 139, 120
Foley R. J., Sanders N. E., Kirshner R. P., 2011, ApJ, 742, 89
Freedman W. L., Madore B. F., Gibson B. K., Ferrarese L., Kelson D. D., Sakai S., Mould J. R., Kennicutt R. C., 2001, ApJ, 553, 47
Gerardy C. L. et al., 2004, ApJ, 607, 391
Goldhaber G. et al., 2001, ApJ, 558, 359
Guy J., Astier P. Nobili S., Regnault N., Pain R., 2005, A&A, 443, 781
Hachinger S., Mazzali P. A., Benetti S., 2006, MNRAS, 370, 299
Hachinger S., Mazzali P. A., Tanaka M., Hillebrandt W., Benetti S., 2008, MNRAS, 389, 1087
Hamuy M., Phillips M. M., Suntzeff N. B., Schommer R. A., Jose M., Smith R. C., Lire P., Aviles R., 1996, AJ, 112, 2438
Hamuy M., Trager S. C., Pinto P. A., Phillips M. M., Schommer R. A., Ivanov V., Suntzeff N. B., 2000, AJ, 120, 1479
Jeffery D. J., Branch D., 1990, in Wheeler J. C., Piran T., Weinberg S., eds, Jerusalem Winter School for Theoretical Physics Vol. 6, Supernovae. World Scientific, Singapore, p. 149
Kehusmaa P., 2009, CBET, 1707, 1
Kirshner R. P. et al., 1993, ApJ, 415, 589
Landolt A. U., 1992, AJ, 104, 340
Leloudas G. et al., 2009, A&A, 505, 265
Li W. et al., 2011, MNRAS, 412, 1441
Lira P., 1995, MSc thesis, Univ. Chile
Lira P., Suntzeff N. B., Phillips M. M., Hamuy M., Maza J., Schommer R. A., Smith R. C., Wells L. A., 1998, AJ, 115, 234
Maeda K. et al., 2010, Nat, 466, 82
Maguire K. et al., 2012, MNRAS, 426, 2359
Mannucci F., Della Valle M., Panagia N., Cappellaro E., Cresci G., Maiolino R., Petrosian A., Turatto M., 2005, A&A, 433, 807
Mannucci F., Della Valle M., Panagia N., 2006, MNRAS, 370, 773
Mazzali P. A., Benetti S., Altavilla G., Blanc G., Cappellaro E., Elias-Rosa N., Garavini G., Goobar A., 2005, ApJ, 623, L37
Mazzali P. A., Sauer D. N., Pastorello A., Benetti S., Hillebrandt W., 2008, MNRAS, 386, 1897
Modjaz M., Li W., Filippenko A. V., King J. Y., Leonard D. C., Matheson T., Treffers R. R., 2001, PASP, 113, 308
Nugent P., Phillips M., Baron E., Branch D., Hauschildt P., 1995, ApJ, 455, L147
Pastorello A. et al., 2007, MNRAS, 376, 1301
Phillips M. M., 1993, ApJ, 413, L105
Phillips M. M., Suntzeff N. B., Hamuy M., Leibundgut B., Kirshner R. P., Foltz C. B., 1992, AJ, 103, 1632

Phillips M. M., Lira P., Suntzeff N. B., Schommer R. A., Hamuy M., Jose M., 1999, AJ, 118, 1766
Pignata G. et al., 2008, MNRAS, 388, 971
Prieto J. L., Rest A., Suntzeff N. B., 2006, ApJ, 647, 501
Pskovskii Y. P., 1984, Sov. Astron., 28, 658
Reindl B., Tammann G. A., Sandage A., Saha A., 2005, ApJ, 624, 532
Riess A. G., Pree W. H., Kirshner R. P., 1996, ApJ, 473, 88
Riess A. G. et al., 1999, AJ, 118, 2675
Sahu D. K. et al., 2008, ApJ, 680, 580
Salvo M. E., Cappellaro E., Mazzali P. A., Benetti S., Danziger I. J., Patat F., Turatto M., 2001, MNRAS, 321, 254
Schlegel D. J., Finkbeiner D. P., Davis M., 1998, ApJ, 500, 525
Silverman J. M., Ganeshalingam M., Li W., Filippenko A. V., 2012, MNRAS, 425, 1889
Sobolev V. V., 1957, Sov. Astron., 1, 678
Stritzinger M., Leibundgut B., 2005, A&A, 431, 423
Suntzeff N. B., 1996, in McCray R., Wang Z., eds, Supernovae and Supernovae Remnants. Cambridge Univ. Press, Cambridge, p. 41
Taubenberger S. et al., 2008, MNRAS, 385, 75
Turatto M., Benetti S., Cappellaro E., Danziger I. J., Della Valle M., Gouiffes C., Mazzali P. A., Patat F., 1996, MNRAS, 283, 1
Turatto M., Benetti S., Cappellaro E., 2003, in Hillebrandt W., Leibundgut B., eds, Proc. ESO-MPA-MPE Workshop, From Twilight to Highlight: The Physics of Supernovae. Springer, Berlin, p. 200
Vinko J., Marion H., Wheeler J. C., Gerardy C., 2009, CBET, 1710, 1
Walker E. S. et al., 2011, MNRAS, 410, 1262
Wang L., Goldhaber G., Aldering G., Perlmutter S., 2003, ApJ, 590, 944
Wang X., Wang L., Zhou X., Lou Y.-Q., Li Z., 2005, ApJ, 620, L87
Wang X. et al., 2009, ApJ, 697, 380
Wells L. A. et al., 1994, AJ, 108, 2233
Yamanaka M., Arai A., 2009, CBET, 1710, 1

This paper has been typeset from a TEX/LATEX file prepared by the author.